Chapter 15: Iron Mineralogy and Aqueous Alteration on Mars from the MER Mössbauer Spectrometers

Richard V. Morris

NASA Johnson Space Center, Houston, TX, USA

and

Göstar Klingelhöfer

Johannes Gutenberg-Universität, Mainz, Germany

ABSTRACT

The twin Mars Exploration Rovers Spirit (Gusev crater) and Opportunity (Meridiani Planum) used MIMOS II Mössbauer spectrometers to analyze martian surface materials in the first application of extraterrestrial Mössbauer spectroscopy. The instruments acquired spectra that identified the speciation of Fe according to oxidation state, coordination state, and mineralogical composition and provided quantitative information about the distribution of Fe among oxidation states, coordination states, and Fe-bearing phases. A total of 12 unique Fe-bearing phases were identified: Fe^{2+} in olivine, pyroxene, and ilmenite; Fe^{2+} and Fe^{3+} in magnetite and chromite; Fe^{3+} in nanophase ferric oxide (npOx), hematite, goethite, jarosite, an unassigned Fe^{3+} sulfate, and an unassigned Fe^{3+} phase associated with jarosite; and Fe^0 in kamacite. Weakly altered basalts at Gusev crater ($SO_3 = 2.5 \pm 1.4$ wt.% and $Fe^{3+}/Fe_T = 0.24 \pm 0.11$) are widespread on the Gusev plains and occur in less abundance on West Spur and Husband Hill in the Columbia Hills. Altered low-S rocks ($SO_3 = 5.2 \pm 2.0$ wt.% and $Fe^{3+}/Fe_T = 0.63 \pm 0.18$) are the most common type of rock in the Columbia Hills. Ilm-bearing, weakly altered basalts were detected only in the Columbia Hills, as was the only occurrence of chromite in an altered low-S rock named Assemblee. Altered high-S rocks ($SO_3 > 14.2$ wt.% and $Fe^{3+}/Fe_T = 0.83 \pm 0.05$) are the outcrop rocks of the ubiquitous Burns formation at Meridiani Planum. Two Fe^0-bearing rocks at Meridiani Planum (Barberton and Heat Shield Rock) are meteorites. Laguna Class soil is weakly altered ($SO_3 = 6 \pm 2$ wt.% and $Fe^{3+}/Fe_T = 0.29 \pm 0.08$) and widely

distributed at both Gusev crater and Meridiani Planum, implying efficient global mixing processes or a global distribution of precursor rocks with comparable Fe mineralogical compositions. Paso Robles Class soil is heavily altered ($SO_3 \sim 31$ wt.% and $Fe^{3+}/Fe_T = 0.83 \pm 0.05$), is relatively uncommon, and occurs as subsurface deposits in the Columbia Hills. Berry Class soil is also heavily altered ($SO_3 = 5 \pm 1$ wt.% and $Fe^{3+}/Fe_T = 0.60 \pm 0.13$) and occurs at Meridiani Planum as lag deposits, at the crests of aeolian bedforms, and as isolated pockets on outcrop surfaces. Magnetite is identified as the strongly magnetic component in martian soil. Jarosite (in the Burns outcrop at Meridiani Planum) and goethite (in Clovis Class rocks at Gusev crater) are mineralogical markers for aqueous processes because they contain the hydroxide anion (OH^-) as an essential part of their structure. Each yields ~10 wt.% H_2O upon dehydroxylation. The presence of Fe sulfates on opposite sides of Mars is evidence that aqueous processes under acid sulfate conditions are or were common. Except for Independence Class rocks in the Columbia Hills, the overall Fe mineralogical compositions and similar basaltic bulk chemical compositions (calculated with respect to $S = Cl = 0$) of the population of altered rocks analyzed by MER imply isochemical alteration of basaltic precursors at low water-to-rock ratios.

1. Introduction

As part of the Athena instrument package, the Mars Exploration Rovers (MER) carried Mössbauer (MB) spectrometers to the surface of another planet for the first time. The rover named "Spirit" landed at Gusev crater on 4 January 2004, and the rover named "Opportunity" landed on the other side of the planet at Merdiani Planum on 24 January, 2004 UTC (Squyres *et al.*, 2004,a,b, 2006; Arvidson *et al.*, 2006). The MER miniature MB spectrometers MIMOS II (Klingelhöfer *et al.*, 2003) detect ^{57}Fe, which has about 2% natural abundance. Mössbauer spectra provide information on the Fe oxidation state (*e.g.*, Fe^0, Fe^{2+}, and Fe^{3+}), the Fe coordination state (*e.g.*, tetrahedral and octahedral coordination), and the relative abundance of Fe among oxidation states, coordination states, and Fe-bearing phases. Identification of oxidation state, coordination state, and Fe-bearing phases are provided by the positions of peaks in a Mössbauer spectrum, and the relative distribution of Fe among oxidation state, coordination

state, and Fe-bearing phases is calculated by summing the areas of peaks (subspectra associated with particular oxidation states, coordination states, and phases).

Mössbauer spectrometers were sent to Mars because the element Fe, which is multivalent and abundant, provides essential geochemical and mineralogical information. Ferrous iron (Fe^{2+}) is common in many rock-forming minerals (*e.g.*, olivine, pyroxene, ilmenite, (titano)magnetite, and chromite) and secondary minerals (*e.g.*, serpentine and sulfates). The ratio of Fe^{3+} to total Fe (Fe^{3+}/Fe_T) for an igneous assemblage is a measure of the prevailing oxygen fugacity during crystallization. Although present at significant levels in some primary phases (*e.g.*, augite and (titano)magnetite), ferric iron (Fe^{3+}) is commonly a product of oxidative alteration and weathering of primary minerals and often occurs as oxides and oxyhydroxides (*e.g.*, hematite and goethite). The speciation and distribution of Fe in martian rock and soil thus constrain the primary rock type (*e.g.*, olivine- versus pyroxene-bearing basalt), the redox conditions under which primary igneous assemblages crystallize, (*e.g.*, presence or absence of magnetite and metallic Fe), the extent of oxidative alteration and weathering (value of Fe^{3+}/Fe_T), the type of alteration and weathering products (*e.g.*, oxides versus sulfates versus phyllosilicates), and the processes and environmental conditions for alteration and weathering (*e.g.*, neutral versus acid-chloride versus acid-sulfate aqueous process under ambient or hydrothermal conditions; Morris *et al.*, 2000).

In this chapter, we first review some of the basic principles of Mössbauer spectroscopy, and then we review and synthesize the Mössbauer results and implications from the first 602 sols (martian days) of Spirit's mission at Gusev Crater and the first 557 sols of Opportunity's mission at Meridiani Planum. Substantial additional details and results and discussion of the implications of the MER Mössbauer investigations can be found in Morris *et al.* (2004, 2006a,b), Klingelhöfer *et al.* (2004, 2006), and Clark *et al.* (2007).

2. Mössbauer spectroscopy and Mössbauer mineralogy on Mars

A full and detailed discussion of the Mössbauer effect and Mössbauer spectroscopy is beyond the scope of this chapter. However, we provide a brief discussion in order to give context for the MER MB results, and the reader is referred to the literature for additional details regarding the Mössbauer effect (*e.g.*, Wertheim, 1964; Wegener, 1966; Greenwood and Gibb, 1971; Bancroft, 1973; Gütlich *et al.*, 1978; Hawthorne, 1988; Burns, 1993).

The Mössbauer effect (also known as recoil-free nuclear gamma resonance absorption) is the recoil-free emission and absorption of gamma rays by nuclei. When the energies of emitting and absorbing nuclei are identical within the line width of the nuclear transition, the resonant absorption process can take place with a certain probability given by the Lamb-Mössbauer factor *f*. The *f*-factor (sometimes called the Debye-Waller factor) is large when the Mössbauer nuclei are bound in solid materials and have relatively low ground-state transition energies. Not all elements have suitable nuclear transitions. The isotope ^{57}Fe (2.2% natural abundance) does have a suitable nuclear transition with an energy difference of 14.41 keV between ground and first excited states. An exact energy match between absorbing and emitting ^{57}Fe nuclei would not occur, even if the *f*-factor is close to maximum (1.0), if the nuclei are in different electronic or magnetic environments or if their speciations (*e.g.*, oxidation, coordination, and mineralogical states) are different. An exact energy match can be made, however, by systematically changing the energy of the emitted or absorbed gamma ray. In laboratory Mössbauer spectrometers, this "energy scanning" is normally accomplished using the Doppler effect, in which the emitter ^{57}Fe nuclei are set in motion relative to the absorber whose position is fixed.

Energy level diagrams and corresponding Mössbauer spectra are shown schematically in Figure 1 for typical situations encountered in the ^{57}Fe Mössbauer spectroscopy of geological materials. The source is chosen to have an "unsplit" 14.41 keV emission line to minimize the complexity of the MB spectra. A commonly used source and the one selected for the MER MB spectrometers is ^{57}Co incorporated into rhodium metal foil (^{57}Co(Rh)). The ^{57}Co decays in part to the first excited state of ^{57}Fe, which decays to the ground state with emission of the 14.41 keV gamma ray or ejection of an atomic electron. The number and position of absorber lines is determined by the symmetry and nature of the surroundings of the ^{57}Fe nuclei. Only one line is obtained (Absorber 1) if no magnetic field is present and the electric field has cubic symmetry. For example, spinel ((Mg,Fe^{2+})Al_2O_4) is a geological material with a singlet Mössbauer spectrum. If the symmetry around the ^{57}Fe nuclei is lowered so that an electric field gradient is present, the nuclear energy levels of the excited state are split so that doublet MB spectra are obtained (Absorber 2). Olivine ((Mg,Fe^{2+})$_2SiO_4$; hereafter denoted as Ol), pyroxene ((Mg,Ca,Fe^{2+})SiO_3; hereafter denoted as Px), and ilmenite ($Fe^{2+}TiO_3$; hereafter denoted as Ilm) are rock-forming minerals that are characterized by doublet MB spectra. In the presence of a magnetic field, both ground- and excited-state ^{57}Fe nuclear energy levels are completely split,

and sextet MB spectra are obtained (Absorber 3). Hematite (α-Fe$_2$O$_3$; hereafter denoted as Hm), goethite (α-FeOOH; hereafter denoted as Gt), magnetite (Fe$_3$O$_4$; hereafter denoted as Mt), troilite (FeS), and kamacite (α-(Fe,Ni)^0 alloy with <8% Ni; hereafter denoted as Kam) are geological materials characterized by sextet MB spectra. Magnetite actually has two sextets, one from Fe^{3+} in the tetrahedral site (tet-Fe^{3+}) and one from Fe^{2+} + Fe^{3+} (denoted as Fe$^{2.5+}$) in the octahedral site (oct-Fe$^{2.5+}$).

   Transmission measurement geometry, where the sample is located between source and detector, is implied by diagrams in Figure 1. The MB peaks project downward from the baseline (100% transmission) because the absorber in each case is located between the MB source and detector. For planetary exploration, however, backscatter measurement geometry, where source and detector are on the same side of the sample, is a better choice because sample preparation is not required. Backscatter geometry was adopted for the MER MIMOS II Mössbauer spectrometers (Klingelhöfer *et al.*, 2003), and the instrument sensor head (Figure 2a) is simply placed in physical contact with martian surface targets by the robotic arm on the MER rovers. Contact is sensed by spring-loaded micro switches that close when the contact plate is depressed as the sensor head encounters the surface. The field of view is 1.5 cm (Figures 2a and 2h). In backscatter geometry, either the 14.41-keV γ-rays or the fluorescent Fe X-rays may be detected following excited-state decay. Only MB spectra derived from the resonantly scattered 14.41 keV γ-rays are discussed here. The peaks project upward from the baseline because the detected radiation is emitted from the sample, and in the case of resonance conditions the intensity of emitted radiation increases. MIMOS II includes an internal velocity calibration standard (α-Fe metal foil + Hm + Mt) measured in transmission geometry simultaneously with surface samples (Klingelhöfer *et al.*, 2003). Fe-bearing phases in rock or soil substrates cannot be detected below ~3 mm of basaltic air-fall dust for the 14.41 keV γ-rays (Morris *et al.*, 2001; Klingelhöfer *et al.*, 2003), and thus brushing or grinding with each rover's Rock Abrasion Tool (RAT) has often been critical in assessing the intrinsic Fe mineralogy at both landing sites.

   The peak positions in MB spectra can be described by three parameters arising from hyperfine interactions between atomic electrons and the ^{57}Fe nucleus: (i) the center shift relative to velocity zero, which is the sum of the isomer (or chemical) shift (δ) and the second order Doppler shift (SODS), a relativistic effect resulting from temperature differences between sample and source; (ii) the quadrupole splitting (ΔE_Q); and (iii) the magnetic hyperfine field (B_{hf})

(Figure 1). The value of δ is a relative number between two materials. To compare δ values, the parameter is referenced to a standard material, and, in keeping with standard practice, we use the center point of the spectrum of α-Fe metal foil for MER MB spectra. In terrestrial laboratories, the source is normally kept at ambient temperature. This produces a temperature dependence of the center shift when the sample temperature is varied with respect to the source at ambient temperature. This temperature dependence is not relevant for MER MB measurements because the sample, source, and internal calibration standard are always at approximately the same temperature, as measured by temperature sensors in the contact plate and within the sensor head (Figure 2a; Klingelhöfer *et al.*, 2003). The temperature of sample, source, and standard all track each other over the duration of a MB integration in response to the martian diurnal temperature cycle. The MER MIMOS II spectrometers measure temperature during MB experiments and record Mössbauer data as a function of temperature in intervals that are 10 K wide (Klingelhöfer *et al.*, 2003).

The MB spectrum of a complex geologic material is a sum of MB subspectra from each distinct Fe site, *i.e.*, sites characterized by different values of the MB parameters. A single Fe-bearing phase can have one or more distinct sites. The subspectra are obtained from the measured MB spectrum using a least squares fitting procedure. The details of the fitting procedures for MER MB spectra are discussed by Morris *et al.* (2006a,b). Mineralogical assignments are made by comparing the subspectral MB parameters to MB parameters that have been compiled for known mineralogical compositions (*e.g.*, Burns and Solberg, 1990; Burns, 1993; McCammon, 1995; Stevens *et al.*, 1998). However, there may be Fe-bearing phases on Mars that are unknown on Earth. Correlations of subspectral areas can also yield clues for mineralogical assignments (*e.g.*, a positive correlation between two subspectral areas might imply that they are present in different sites in the same Fe-bearing phase). In any case, mineralogical assignments on the basis of MB data must be examined within the context of other MER chemical and mineralogical data (*e.g.*, Gellert *et al.*, 2004, 2006; Rieder *et al.*, 2004; Christensen *et al.*, 2004a,b; Ming *et al.*, 2006; Yen *et al.*, 2006) and what is known about the environment and geochemistry of Mars.

The percentage of total Fe associated with a specific Fe-bearing phase (A_x where $\Sigma A_x = 100\%$) is determined by its subspectral area corrected for the recoil-free fraction (the *f*-factor) of ^{57}Fe in that phase. For MER, we use $f(Fe^{2+})/f(Fe^{3+}) = 1.21$, independent of mineralogical

composition (De Grave and Van Alboom, 1991; Morris *et al.*, 1995). Note that A_x is the percentage of total iron associated with a particular Fe-bearing phase and not the concentration of the Fe-bearing phase in a sample. Thus, for example, a sample can be 100% olivine as forsterite (Mg_2SiO_4) but have 0% olivine with respect to MB measurements because forsterite contains no Fe.

In summary, the information content of "Mössbauer mineralogy" is the oxidation and coordination states of Fe, the mineralogical composition of Fe-bearing phases, and the distribution of Fe among oxidation states, coordination states, and Fe-bearing phases. In practice, it is relatively straightforward to determine the Fe oxidation state (Fe^{3+}/Fe_T) from MB data, but more challenging to assign specific mineralogical compositions to Fe-bearing phases.

3. Identification and mineralogical assignment of Fe-bearing phases

The MB doublet (δ versus ΔE_Q) and sextet (δ versus ΔE_Q and δ versus B_{hf}) identification diagrams are shown in Figure 3 for MER MB data through sols 602 and 575 at Gusev crater and Meridiani Planum, respectively. The parameters were derived from fits of spectra that are the sum of individual spectra from temperature windows between 200 and 270 K (Morris *et al.*, 2006a,b). We give each Fe-bearing phase a generic name having the form FeXYZ, where X = Fe oxidation state, Y = D (doublet) or S (sextet), and Z = a sequence number for phases with the same values of X and Y. A total of 9 doublets and 5 sextets, corresponding to 12 distinct Fe-bearing phases, were identified on Mars. We briefly summarize mineralogical assignments next. Additional details can be found in Morris *et al.* (2004, 2006,a,b), Klingelhöfer *et al.* (2004), and Clark *et al.* (2007).

Doublets Fe2D1, Fe2D2, and Fe2D3 (Figure 3a) are assigned to octahedrally coordinated Fe^{2+} (oct-Fe^{2+}) in olivine (Ol), pyroxene (Px), and ilmenite (Ilm), respectively, on the basis of comparison to MB parameters compiled in databases (*cf.*, section 2). The assignments for Ol and Px are consistent with MER Mini-TES data (*e.g.*, Christensen *et al.*, 2004a). Although the MB parameters for Fe2D1 are consistent with Fe in Ol, an alternate assignment of Fe^{2+}-bearing sulfate was made by Lane *et al.* (2004) for Fe2D1, implying that the Fe2D1 parameters are not specific for Ol. As discussed by Yen *et al.* (2005) and Morris *et al.* (2006a), the sulfate assignment is unlikely because of the aforementioned Mini-TES data, the observed decreasing A_{Ol} with increasing SO_3 concentration, and, for rock interiors exposed by grinding with the RAT,

SO_3 concentrations that are too low to accommodate all Fe from Fe2D1 as an Fe^{2+}-bearing sulfate. Ilmenite was not detected by mini-TES, but samples that have Ilm as detected by MB also have higher TiO_2 concentrations as detected by APXS (*e.g.*, Gellert *et al.*, 2004, 2006; Ming *et al.*, 2006). Doublets Fe3D1, Fe3D2, and Fe3D4 (Figure 3c) are assigned to oct-Fe^{3+} in nanophase ferric oxide (npOx), an unidentified Fe^{3+} sulfate (Fe3Sulfate), and jarosite (Jar), respectively. The jarosite ($(K,Na,H_3O)(Fe,Al)_3(SO_4)_2(OH,Cl)_6$ where Fe > Al and OH > Cl) assignment is made on the basis of the unusually high value of ΔE_Q for that phase. The assignment of Fe^{3+}-sulfate is based on the relatively high value of δ and S concentrations that are so high ($SO_3 \sim 31$ wt.%) that they require nearly all cations to occur as sulfates. The npOx refers to a poorly crystalline or amorphous alteration product that can be any combination of superparamagnetic hematite and/or goethite, akaganeite (β-FeOOH), schwertmannite ($\sim Fe_8O_8(OH)_6SO_4$), ferrihydrite ($5Fe_2O_3 \bullet 9H_2O$), iddingsite (a low-temperature alteration product of olivine), and the nanometer-sized ferric oxide particles that pigment palagonitic tephra (*e.g.*, Morris *et al.*, 1993, 2000). NpOx can also incorporate anions (*e.g.*, SO_4^{2-} and PO_4^{3-}) through specific chemical adsorption (*e.g.*, Borggaard, 1983a,b; Cornell and Schwertmann, 1996; Myneni, 2000). The nature of npOx can change from place-to-place and time-to-time, in response to local conditions and processes. Thus, it is possible that the form of npOx on Mars is uncommon or not present on the Earth.

Sextets Fe3S1, Fe2.5S1, Fe3S2, Fe3S3, and Fe0S1 are assigned to tet-Fe^{3+} in magnetite, oct-$Fe^{2.5+}$ in magnetite, oct-Fe^{3+} in hematite, oct-Fe^{3+} in goethite, and Fe^0 in kamacite, respectively (Figure 3b). The envelope for Hm data is large compared to the other sextet phases because Hm undergoes a magnetic transition (the Morin transition) within the martian diurnal temperature cycle (~180 to 300 K). For well crystalline and chemically pure hematite, this transition occurs at $T_M \sim 260$ K, where $\Delta E_Q < 0$ for $T > T_M$ and $\Delta E_Q > 0$ for $T < T_M$. For Hm with small particle sizes and/or with substitutional impurities like Al, the Morin transition occurs at lower temperatures and over a wider temperature interval (*e.g.*, De Grave *et al.*, 1983, 2002). Small-particle behavior and/or substitutional impurities are indicated for most martian hematites because $\Delta E_Q < 0$ mm/s at martian diurnal temperatues (Figure 3b and Morris *et al.*, 2006a).

In summary, 9 doublets and 5 sextets were identified in MER MB spectra through sols 602 and 557 at Gusev crater and Meridiani Planum, respectively. Specific mineralogical assignments were made for 5 of 9 doublets (Fe^{2+} in Ol, Px, and Ilm; Fe^{3+} in npOx and Jar) and

for all 5 sextets ($Fe^{2.5+}$ and Fe^{3+} in Mt; Fe^{3+} in Hm and Gt; Fe^0 in Kam). One doublet (Fe3D2) is associated with oct-Fe^{3+} in a sulfate, but we cannot assign a specific Fe^{3+}-sulfate mineral. Two doublets (Fe2D4 and Fe3D5) are associated with chromite ($Fe^{2+}(Cr,Fe^{3+})_2O_4$ where $Cr > Fe^{3+}$; hereafter denoted as Chr), but this association would not have been possible to make without knowledge of high Cr concentrations in the sample from APXS measurements. We make no specific mineralogical assignment for the final doublet (Fe3D3), except that it results from a phase with oct-Fe^{3+}. In Figure 4, we show MER MB spectra for samples that contain high proportions of each of the 14 doublets and sextets identified in 12 unique Fe-bearing phases. Average values of doublet and sextet MB parameters for individual Fe-bearing phases are summarized in Tables 1 and 2, respectively.

4. Supergroup classification of MER rocks and soils

In Figure 5, we show the frequency of occurrence of the unique 12 Fe-bearing phases for rocks and soils at Gusev Crater and Meridiani Planum. The histograms count only those occurrences in MB spectra where the abundance of Fe from an Fe-bearing phase is >10% (*i.e.*, $A_x > 10\%$). We counted all distinct measurements of the same target as separate occurrences. The total number of occurrences of each phase is indicated in the figure.

Five phases have very limited occurrence in MER MB spectra. Chromite is present only in Gusev Columbia Hills rock sample Assemblee_Guryere. Fe^{3+}-sulfate occurs only in two Gusev Columbia Hills soil analyses (Pasadena_PasoRobles and PasoRobles2_PasoLight1). Ilmenite is found in rocks and one soil in the Columbia Hills. Goethite is detected only in rocks from the Columbia Hills. Kamacite occurs only at Meridiani Planum in Heat Shield Rock and in the cobble sample Figtree_Barberton.

The Fe mineralogical composition of rocks at Gusev crater is very different from those at Meridiani Planum (Figures 5a, 5c). Fe-bearing phases associated with igneous rocks (Ol, Px, Mt, Ilm, and Chr) are prevalent at Gusev crater. The Gusev rocks with Hm >10% and Gt >10% are confined to the Columbia Hills and do not occur on the plains. Rock analyses at Meridiani Planum are dominated by measurements of the ubiquitous high-S Burns formation (Rieder *et al.*, 2004; Grotzinger *et al.,* 2005), which is an assemblage of Jar, Hm, and Fe3D3 with respect to Fe-bearing phases (Morris *et al.,* 2006b). The Hm occurs both within the Hm-rich spherules and within the matrix of sulfate-rich rock at particle diameters below the resolution of the MER

Microscopic Imager (Morris *et al.*, 2006b). This result is consistent with Pancam multispectral imaging of the outcrop rocks (Bell *et al.*, 2004b). The high number of pyroxene analyses at Meridiani Planum is inflated by the eight MB analyses of Bounce Rock, the most Px-rich sample measured at either MER site.

Compared to rocks, the Fe mineralogical composition of soils at Gusev Crater and Meridiani Planum is less variable (Figures 5b and 5d), although Mt is relatively common compared to Hm at Gusev crater and vice versa for Meridiani Planum. This difference may reflect the prevalence at Gusev and apparent absence at Meridiani of Mt-bearing rocks, and the abundance of Hm-rich spherules at Meridiani Planum. We next consider the distribution of Fe-bearing phases within individual rocks and soils and classify them into supergroups on the basis of chemistry and Fe mineralogy (Table 3).

In order to do this classification, we take into account that two or more samples can have identical distributions of Fe among Fe-bearing phases and yet have different bulk elemental compositions. For example, two rocks can both have $A_{Ol} = 40\%$, $A_{Px} = 35\%$, $A_{Mt} = 15\%$, and $A_{npOx} = 10\%$ but very different total Fe concentrations (Fe_T) if they have different proportions of phases that have virtually no Fe (*e.g.*, plagioclase). We use parameters of the form $A_{Ol}Fe_T/100$ (using olivine as an example) to classify soils and rocks into supergroups. The "100" in the denominator is necessary because A_{Ol} is a percentage. We calculate $A_{Ol}Fe_T/100$ in units of moles per 24 moles of oxygen plus chlorine (moles/24(O+Cl)) because stoichiometric information is directly accessible with molar concentration units. We use "24(O+Cl)" because 24 is evenly divisible by the sum of oxygen plus chlorine for many common geological materials (*e.g.*, Fe_2SiO_4, $FeSiO_3$, Fe_3O_4, Fe_2O_3, and $FeTiO_3$). Note that this classification is based on both mineralogical (A_{Ol}, A_{Px}, etc. from MB) and elemental (Fe_T from APXS) data (Gellert *et al.*, 2004; Rieder *et al.*, 2004; Morris *et al.*, 2006a,b; Yen *et al.*, 2006).

We divided the rocks into four supergroups: Weakly Altered Basalt, Altered Low-S Rock, Altered High-S Rock, and Meteorite. The Meteorite supergroup consists of the two rocks from Meridiani Planum that have kamacite as an Fe-bearing phase (Heat Shield Rock and the cobble Barberton). We used plots of Fe_T and S as a function of four parameters having the form $A_xFe_T/100$ to classify the remaining MER rocks into supergroups (Figure 6). The parameter (A_{Ol} + A_{Px} + A_{Ilm} + A_{Chr} + A_{Mt})$Fe_T/100$ (equivalently $A_{Igneous}Fe_T/100$) is the sum of Fe concentrations from igneous, rock-forming phases. Samples that plot on or near the y = x line in Figures 6a are

potentially unaltered samples. However, rocks with high concentrations of Fe from Ilm and Chr resulting from alteration of a precursor basalt with those minerals would also plot along this line, except at lower values of Fe_T because of removal of Fe (*e.g.*, by leaching) from Fe-bearing phases that are susceptible to alteration (*e.g.*, Ox and Px). We classify the group of rocks with high values of Fe_T ($Fe_T > 1.2$ moles/24moles(O+Cl)) and $Fe_T \approx A_{Igneous}Fe_T/100$ as "Weakly Altered Basalt" as shown in Figure 6a. Weakly Altered Basalt at Gusev crater has $S = 0.28 \pm 0.15$ moles/24(O+Cl) ($SO_3 = 2.5 \pm 1.4$ wt.%) and $Fe^{3+}/Fe_T = 0.24 \pm 0.11$. The values for S and SO_3 exclude the rocks Peace and Alligator, which have a Mg-sulfate coating and/or cement (Ming *et al.*, 2006) but are still Weakly Altered Basalt with respect to Fe-bearing phases.

The parameters $(A_{Jar} + A_{Fe3D3} + A_{Hm})Fe_T/100$ and $A_{Hm}Fe_T/100$ are, respectively, the sum of Fe^{3+}-bearing alteration products associated with the Burns formation and the Fe concentration from Hm. Altered High-S Rock from the Burns formation is distinguished from Altered Low-S Rock and Weakly Altered Basalt in Figures 6b and 6c. Weakly Altered Basalt and Altered Low-S Rocks have S concentrations between 0 and ~1.5 moles/24(O+Cl) (equivalently, 0 to ~14.2 wt.% SO_3), and Altered High-S Rock has S concentrations greater than ~1.5 moles/24(O+Cl) (>14.2 wt.% SO_3) (Figure 6c). Altered Low-S basalt has average $S = 0.55 \pm 0.21$ moles/24(O+Cl) ($SO_3 = 5.2 \pm 2.0$ wt.%) and $Fe^{3+}/Fe_T = 0.63 \pm 0.18$. In general, Altered High-S Rock has higher Hm concentrations than Altered Low-S Rock (Figure 6d). In Figures 6b, 6c, and 6d, Weakly Altered Basalt plots on or near the y-axis.

As shown in Figure 6c, some measurements of Burns outcrop targets have S concentrations less than ~1.5 moles/24(O+Cl), which is in the range for Altered Low-S Rock. The low S concentrations result from thin coverings of low-S Laguna Class soil (discussed below) that are "thick" with respect to APXS analysis and "thin" with respect to MB analysis (Morris *et al.*, 2006b). All APXS measurements of outcrop surfaces exposed by the MER RAT have sulfur concentrations greater than 1.5 moles/24(O+Cl) (Figure 6c). Including only analyses of RAT-ground surfaces, Altered High-S Rock has average $S = 2.27 \pm 0.26$ moles/24(O+Cl) ($SO_3 = 22 \pm 3$ wt.%) and $Fe^{3+}/Fe_T = 0.85 \pm 0.03$.

For each rock supergroup, average values of the concentrations of Fe associated with Fe-bearing phases $(A_xFe_T/100)$, Fe_T and S concentrations, Fe^{3+}/Fe_T, and number of targets with both APXS and MB analyses are summarized in Table 3. Individual rocks are classified according to

supergroup, APXS chemistry (*e.g.*, Squyres *et al.*, 2006; Ming *et al.*,2006), and MB mineralogy (Morris *et al.*, 2006,a,b) in Table 4.

We divided MER soils into three supergroups on the basis of Figure 7: Laguna Class (LC) supergroup, Paso Robles Class (PRC) supergroup, and Berry Class (BC) supergroup. Paso Robles Class soils have the lowest values of $A_{Igneous}Fe_T/100$ (Figure 7a), and they have the highest S concentrations measured on Mars to date (Figures 6c and 7c). Paso Robles Class soils have average S = 3.17 ± 0.04 moles/24moles(O+Cl) (SO_3 = 31.1 ± 0.1 wt.%) and Fe^{3+}/Fe_T = 0.83 ± 0.05. Laguna Class soils plot near the y = x line in Figure 7a and thus (for soils) have the highest proportions of igneous rock forming minerals and are the least altered with average S = 0.66 ± 0.24 moles/24moles(O+Cl) (SO_3 = 6 ± 2 wt.%) and Fe^{3+}/Fe_T = 0.29 ± 0.08. Comparison of Figures 6a and 7a shows that the Weakly Altered Basalt rock supergroup and the Laguna Class soil supergroup have comparable values of Fe_T and $A_{Igneous}Fe_T/100$. Berry Class soils, which have values of $A_{Igneous}Fe_T/100$ comparable to Laguna Class soils (Figure 7a), are distinguished by the high values of Fe_T and by high values of $A_{Hm}Fe_T/100$ (Figures 7a and 7d) that result from high concentrations of Hm-rich and Fe-rich spherules and their fragments (Morris *et al.*, 2006b). Note that two Berry Class soils (circled in Figures 7a and at the left side of the ellipse enclosing the BC supergroup) are very similar and transitional to Laguna Class soil. Berry Class soils have average S = 0.61 ± 0.07 moles/24moles(O+Cl) (SO_3 = 5 ± 1 wt.%) and Fe^{3+}/Fe_T = 0.60 ± 0.13. Comparison of Figures 7b and 7d shows that no soil has detectable Fe from Jar and Fe3D3.

Average values of the concentrations of Fe associated with Fe-bearing phases ($A_xFe_T/100$), Fe_T and S concentrations, Fe^{3+}/Fe_T, and number of targets with both APXS and MB analyses for each soil supergroup are summarized in Table 3. Individual soils are classified according to supergroup and APXS chemistry and MB mineralogy in Table 5 (after Morris *et al.*, 2006,a,b).

Morris *et al.* (2006a) defined a Mineralogical Alteration Index (MAI = $A_{Alteration}$ = A_{npOx} + A_{Hm} + A_{Gt} + $A_{Fe3Sulfate}$ + A_{Jar} + A_{Fe3D3}) to describe the degree of alteration of Gusev crater rocks. The index, however, is not sensitive to alteration in situations like those for the Independence Class rocks, where alteration and subsequent leaching appear to have resulted in a net loss of Fe from relatively soluble phases (*e.g.*, Ol and Px) and a resulting passive enrichment in Fe associated with less soluble phases (Ilm and Chr). Using data from Clark *et al.* (2007), the

values of MAI for the rocks Assemblee and Independence are 32 % and 43%, respectively. While these values are larger than those for Weakly Altered Basalt (MAI < 22%), they are very low compared to corresponding values for other heavily altered Columbia Hills rocks (*e.g.*, 83%, 88%, and 94% for Watchtower, Pequod, and Paros, respectively). One might instead consider using $A_{Alteration}Fe_T/100$ as a measure of alteration because it explicitly takes in account both Fe from alteration phases and Fe loss from leaching. However, this is not a viable alternative because Weakly Altered Basalts and Independence Class rocks have comparable values of $A_{Alteration}Fe_T/100$.

A different way to look at the degree and type of alteration of MER samples is through plots of $A_{Igneous}Fe_T/100$ versus $A_{Alteration}Fe_T/100$ (Figure 8). The two solid lines at 2.24 and 1.80 moles/24(O+Cl) are, respectively, the average values of Fe_T for Weakly Altered Basalt from Gusev crater and Meridiani Planum. Isochemical alteration of a basalt with $Fe_T = A_{Igneous}Fe_T/100$ = 2.24 (or 1.80) moles/24(O+Cl) and with $A_{Alteration}Fe_T/100 = 0.0$ moles/24(O+Cl) as its initial composition proceeds down the $Fe_T = 2.24$ (or 1.80) moles/24(O+Cl) line toward the $A_{Alteration}Fe_T/100$ axis. Incorporation of SO_3 from acid-sulfate solutions or vapors to form sulfate-bearing phases during alteration would result in rock compositions that plot to the left of the line. Thus, weakly altered Bounce Rock does not appear to be the precursor (by isochemical alteration) of the S-rich outcrop rocks at Meridiani Planum, even though both plot along the line with $Fe_T = 1.80$ moles/24(O+Cl) (Figure 8a). Incorporation of H_2O or OH^{-1} would not be detected because APXS analyses are calculated on an H_2O-free basis. Alteration of a basalt with an initial composition $Fe_T = A_{Igneous}Fe_T/100 = 2.24$ moles/24(O+Cl) in an open system with removal of all oxidized iron (*e.g.*, by leaching) results in a composition on the $A_{Igneous}Fe_T/100$ axis with a value between 0 and 2.24 moles/24(O+Cl). Independence Class rocks are thus likely case where leaching has been important (Figure 8a). Soils at Gusev crater and Meridiani Planum do not appear to be derived directly by isochemical alteration of Weakly Altered Basalt analyzed at the two landing sites (compare Figures 8a and 8b).

In Figure 9 we use pie diagrams to show the average distribution of Fe in Fe-bearing phases for supergroups of rock (Weakly Altered Basalt, Altered Low-S Rock, and Altered High-S Rock) and soil (Laguna Class soil, Paso Robles Class soil, and Berry Class soil) at Gusev Crater and Meridiani Planum. The percentages of Fe in Fe-bearing phases can be calculated from the data in Table 3. Average Weakly Altered Basalt at Gusev crater ($Fe^{3+}/Fe_T = 0.24$) has nearly

equal proportions of Fe from Ol and Px (A_{Ol} + A_{Px} = 71%), nearly equal proportions of Fe from Mt and npOx (A_{Mt} + A_{npOx} = 27%) and possible minor Fe from Hm (1%). Bounce Rock is the only Weakly Altered Basalt at Meridiani Planum (Fe^{3+}/Fe_T = 0.01), and it is essentially monomineralic pyroxene with respect to Fe-bearing phases (A_{Px} = 99%). Average Altered Low-S Rock at Gusev crater (Fe^{3+}/Fe_T = 0.63) has high proportions of Fe^{3+}-only phases (npOx + Hm + Gt = 57%) and much lower Ol + Px (A_{Ol} + A_{Px} = 30%) compared to average Weakly Altered Basalt. Altered Low-S Rock has not been analyzed at Meridiani Planum as of sol 557. Average Altered High-S Rock at Meridiani Planum (Burns formation outcrop rock; Fe^{3+}/Fe_T = 0.85) is heavily dominated by Fe^{3+}-only phases (Jar + Hm + Fe3D3 = 85%). Altered High-S Rock has not been detected at Gusev crater as of sol 602.

Average Laguna Class soil is very similar at Gusev crater (Fe^{3+}/Fe_T = 0.30) and Meridiani Planum (Fe^{3+}/Fe_T = 0.28) in terms of the mineralogy and abundance of Fe from Fe bearing phases (Figure 9d). This suggests mixing, presumably by aeolian processes, on a global scale and/or similar precursor rocks on a global scale. Laguna Class soil is similar in mineralogical composition to Weakly Altered Basalt at Gusev crater. Average Paso Robles Class soil (Fe^{3+}/Fe_T = 0.83) has high proportions of Fe from Fe3Sulfate (A_{Fe3D2} = 65%) plus Hm (A_{Hm} = 14%) and silicates (A_{Ol} + A_{Px} = 16%). Paso Robles Class soil has not been detected at Meridiani Planum. Average Berry Class soil (Fe^{3+}/Fe_T = 0.60) has high proportions of Fe from Hm (A_{Hm} = 44%) plus Fe from silicates (A_{Ol} + A_{Px} = 39%) and Mt and npOx (A_{Mt} + A_{npOx} = 16%). Berry Class soil is likely a mechanical mixture of Hm-rich spherules (and their fragments) and Laguna Class soil. Setting A_{Hm} to 4% for Berry Class soil and recalculating to 100% gives a composition (A_{Ol} = 32%, A_{Px} = 37%, A_{Mt} = 5%, A_{npOx} = 23%, and A_{Hm} = 4%) that is nearly the same as the average for Laguna Class soil at Meridiani Planum (Figure 9d). Berry Class soil has not been detected at Gusev crater as of sol 602.

5. Spatial distribution of rock and soil supergroups

Together with the Fe^{3+}/Fe_T ratio, the analysis locations for the four rock and three soil supergroups are shown in Figure 10 using sol number as a proxy for location. For Gusev crater (Figures 10a and 10c), Weakly Altered Basalt was analyzed on the Gusev plains (rocks Adirondack, MimiShoe, Humphry, Mazatzal, Route66, and Joshua) and on Husband Hill in the Columbia Hills (rocks Peace, Alligator, Backstay, and Irvine). All these rocks are float (*i.e.*,

delivered to their present location rather than formed in place), except for Peace and Alligator which are outcrop rocks. Although Peace and Alligator are Weakly Altered Basalt according to MB analyses, they are enriched in Mg and S suggesting that they were invaded and cemented by Mg-sulfate solutions after formation (*e.g.*, Squyres *et al.*, 2006; Ming *et al.*, 2006). The oxidation state (Fe^{3+}/Fe_T) of Weakly Altered Basalt is largely controlled by magnetite. The rock Route66, with no detectable magnetite, has $Fe^{3+}/Fe_T = 0.07$, and the rocks MimiShoe, Peace, and Irvine, which have significant concentrations of magnetite, have $Fe^{3+}/Fe_T = 0.30$-0.43 (Morris *et al.*, 2006a). CIPW normative mineral calculations for Weakly Altered Basalt from APXS chemistry and MB Fe^{3+}/Fe_T are discussed by McSween *et al.* (2004, 2006). Normative minerals represent the minerals that might crystallize if a rock cooled under equilibrium and anhydrous conditions.

Altered Low-S Rock was analyzed throughout the Columbia Hills. For the most part, the rocks are outcrops (*e.g.*, Wooly Patch, Clovis, and Ebenezer; Squyres *et al.*, 2006). Clovis at West Spur has the highest measured concentration of goethite ($A_{Gt} = 37\%$). Other Gt-bearing rocks with $A_{Gt} > 10\%$ are Ebenezer, Temples, Tetl, Uchben, Lutefisk, Champagne, Watchtower, Paros, and Pequod. Altered Low-S Rock tends to have higher values of Fe^{3+}/Fe_T compared to Weakly Altered Basalt (0.87 and 0.94 for Clovis and Watchtower, respectively), but this is not always the case. For example, Altered low-S outcrop rocks Independence and Assemblee have low values of Fe^{3+}/Fe_T (0.30 and 0.35, respectively) because the Fe associated with primary silicate minerals was removed (presumably by leaching), leaving the oxides Ilm and Chr (Clark *et al.*, 2007).

Laguna Class soil was analyzed throughout the Gusev Plains and the Columbia Hills (average $Fe^{3+}/Fe_T = 0.30$) as undisturbed surface soils and as subsurface soils revealed by trenching or other rover wheel actions. The two Paso Robles Class soils were detected and analyzed on Husband Hill; they are very oxidized ($Fe^{3+}/Fe_T = 0.83$). Paso Robles Class soil occurs in the subsurface, under a thin overburden of Laguna Class soil (see, *e.g.*, Chapter 13 by Bell *et al.*). Thus, its overall geographic extent is unknown because it cannot be detected from martian orbit or by Spirit without disturbing the surface layer.

For Meridiani Planum (Figures 10b and 10d), the rock population is dominated by Altered High-S Rock belonging to Burns Outcrop Class (the Burns formation). The Burns formation rocks are highly oxidized and have Hm-rich spherules dispersed throughout the S-rich rock. The spherules are popularly known as "blueberries" and have been interpreted to be

concretions (Squyres *et al.*, 2004, 2006; Grotzinger *et al*., 2005). The oxidation state (Fe^{3+}/Fe_T = 0.85) and the Fe mineralogical composition of the outcrop (Figure 9c) actually pertain to "interspherule" regions, because spherules were not present in the MB analysis volume. No Altered Low-S Rock and only one Weakly Altered Basalt (Bounce Rock) have been identified by the Opportunity rover at Meridiani Planum through sol 557. An iron meteorite with kamacite (Heat Shield Rock) was analyzed, and Barberton is also a meteorite based on the presence of kamacite (Morris *et al.*, 2006b). Bounce Rock, Heat Shield Rock, and Barberton are regarded as "erratics" within the part of Meridiani Planum explored to date by the rover.

Laguna Class soil at Meridiani Planum (average Fe^{3+}/Fe_T = 0.28) covers the surface of the Burns formations as aeolian bedforms (small ripples and dunes), except for areas of outcrop exposed by impact events (*e.g.*, Eagle, Fram, and Endurance Craters) and in scattered exposed patches in shallow fractures and between bedforms. Berry Class soil, which is composed of basaltic clasts, spherules, and spherule fragments, primarily occurs as a lag deposit at ripple crests or in topographic lows. The cover of Laguna and Berry Class soils over the Burns formation masks its detection from martian orbit (*e.g.*, Bell *et al.*, 2004b; Arvidson *et al.*, 2006). Berry Class soil is the source of the coarse-grained "grey" hematite first detected from martian orbit by the Mars Global Surveyor Thermal Emission Spectrometer (Christensen *et al.*, 2000, 2001) and is thus the mineralogical beacon that focused attention on Meridiani Planum as a MER landing site (*e.g.*, Golombek *et al.*, 2003).

6. NpOx, S, and Cl in martian soil and dust

We discussed earlier the assignment of the oct-Fe^{3+} doublet Fe3D1 to npOx, which is a generic name for a poorly crystalline (probably X-ray amorphous) alteration product with oct-Fe^{3+} as the Fe cation. The concentration of Fe from npOx ($A_{npOx}Fe_T/100$) in Laguna Class and Berry Class martian soils is highly variable (Figure 11), ranging from ~0.2 moles/24(O+Cl) at one extreme (*e.g*., samples BearPaw_Panda, and Crumble_Almonds at Gusev Crater) to ~0.8 moles/24(O+Cl) at the other extreme (*e.g.*, samples Desert_Gobi, Bighole_RS2, and Wymper at Gusev Crater and MontBlanc_LesHauches, Pergatory_Track2, and BigDig_HemaTrench1 at Meridiani Planum). Undisturbed (by rover wheels) surface soils that are bright (high albedo) in Pancam observations (Bell *et al.*, 2004a) and have high dust signatures according to mini-TES (Christensen *et al.*, 2004) characteristically have high values of $A_{npOx}Fe_T/100$ (*e.g.*, samples

Desert_Gobi, Wymper, MontBlanc_LesHauches, and Pergatory_Track2). Disturbed soils (except Paso Robles Class soil) and undisturbed soils that are dark and have low dust signatures characteristically have low values of $A_{npOx}Fe_T/100$ (*e.g.*, sample BearPaw_Panda). These associations imply that martian dust, in addition to being bright and fine grained, has high concentrations of npOx, perhaps higher than for any soil that has been analyzed by MB to date (Morris *et al.*, 2006a,b).

In Figure 11a, we plot the concentration of S as a function of $A_{npOx}Fe_T/100$ for Laguna and Berry Class soils (after Yen *et al.*, 2005; Morris *et al.*, 2006a,b). We also include analyses for two thick dust coatings on the Gusev crater rock Mazatzal (samples Mazatzal_NewYork and Mazatzal_Oregon) (Morris *et al.*, 2006a). The solid line is the linear least squares fit of the data excluding the two analyses of subsurface soils from the Boroughs trench. The trench analyses were excluded because they have anonymously high concentrations of Mg and S, indicating the presence of a Mg-sulfate that is not present in the other soils (Wang *et al.*, 2006a). Figure 11b is the corresponding plot for Cl, and the solid line is the linear least squares fit for all the data. The equations for the fits are given in Figure 11.

A simple explanation of the data in Figure 11 is that the soils are binary mixtures of two endmembers. One endmember, which has the lowest concentrations of $A_{npOx}Fe_T$, S, and Cl, is the composition represented by the y-intercepts of the linear least squares fits ($A_{npOx}Fe_T/100 = 0.0$ moles/24(O+Cl)), *i.e.*, 0.37 and 0.12 moles/24(O+Cl) for S and Cl, respectively. The second endmember is an altered soil having concentrations of S, Cl, and $A_{npOx}Fe_T/100$ extrapolated along the least-squares lines to a value of $A_{npOx}Fe_T/100$ greater than 0.84 moles/24(O+Cl), the highest value observed for that parameter. The upper limit for $A_{npOx}Fe_T/100$ is Fe_T, which is ~2.0 moles/24(O+Cl) for Laguna Class soil at Gusev crater (Figure 7a). The corresponding upper limit concentrations for S and Cl are 1.6 and 0.36 moles/24(O+Cl), respectively. The molar S/Cl ratio depends on $A_{npOx}Fe_T/100$, ranging from 3.1 for $A_{npOx}Fe_T/100 = 0$ moles/24(O+Cl) to 4.4 for $A_{npOx}Fe_T/100 = 2.0$ moles/24(O+Cl).

The slopes in Figure 11 give molar $S/(A_{npOx}Fe_T/100)$ and $Cl/(A_{npOx}Fe_T/100)$ ratios (0.62 and 0.12, respectively) that are potentially characterizing parameters for npOx. Molar S/Fe ratios for typical terrestrial ferric sulfates are 0.13 to 0.25 for schwertmannite, 0.67 for jarosite, 1.5 for binary Fe-sulfates ($Fe_2(SO_4)_3 \cdot nH_2O$), and 1.3 for ferricopiapite ($Fe_{4.67}(SO_4)_6(OH)_2 \cdot 20H_2O$). Although the observed value of the S/Fe molar ratio for npOx is comparable to the value for

jarosite, we believe that the correspondence is a coincidence and not causative evidence for jarosite because (a) the quadrupole splitting (average ± 1σ) for npOx in soils is too low (0.91 ± 0.07 mm/s) compared to 1.20 ± 0.02 mm/s for Meridiani Planum jarosite (Morris *et al.*, 2006b); (b) the molar S/Fe and Cl/Fe ratios are actually upper limits; and (c) reflectivity spectra do not provide a mineralogical constraint for jarosite. With regard to (b), the previous discussion assumes that all S and Cl are associated with npOx. The actual S/Fe and Cl/Fe ratios for npOx would be lower in a scenario where npOx and one or more S- and Cl-bearing and Fe-free phases are formed contemporaneously in fixed proportions during weathering. With regard to (c), multispectral Pathfinder IMP and MER Pancam visible to near-IR data (0.40 – 1.1 μm) and hyperspectral OMEGA near-IR data (1.0 - 2.5 μm) for martian bright regions show a relatively featureless ferric absorption edge extending from ~0.40 to ~0.75 μm and relative constant reflectivity from ~0.75 to 2.5 μm. These spectral characteristics imply npOx and not a jarosite-like phase (*e.g.*, Morris *et al.*, 2000; Bell *et al.*, 2000, 2004; Bibring *et al.*, 2006). According to Bibring *et al.* (2006), the absence of detectable spectra features near 1.4, 1.9, and 2.1-2.4 μm in OMEGA spectra imply that the surface material in martian bright regions (dust or bright soil) is anhydrous. Specifically, a spectral feature associated with the Fe-OH vibration of jarosite (or any other phase with the Fe-OH functional group) was not detected, although the presence of a spectral feature near 3 μm implies that some H_2O/OH must be present (*e.g.*, Yen *et al.,* 1998).

Would we expect to find surface deposits of dust (bright soil) with $A_{npOx}Fe_T/100 = Fe_T$? That is, might there be a high-albedo soil with npOx as the only Fe-bearing phase, with Fe, S, and Cl concentrations of ~2.0, 1.6, and 0.36 moles/24(O+Cl), and with a featureless ferric absorption edge at visible wavelengths? Although possible, such an occurrence is unlikely based on MB spectra of atmospheric dust collected by the MER permanent magnets, which revealed Fe from Ol, Px, and Mt, as well as npOx, in the airborne dust (*e.g.*, Goetz *et al.*, 2005).

7. Mineralogical evidence for aqueous activity on Mars

Although the MER Mössbauer spectrometers are not directly sensitive to either the H_2O molecule or to the hydroxide anion (OH^{-1}), they did identify two Fe bearing phases that have OH^{-1} as a part of their structure and thus did provide direct mineralogical evidence for aqueous activity on Mars. First, goethite (α-FeOOH) is present at Gusev crater in a series of outcrop rocks (Clovis Class) on Husband Hill (Morris *et al.*, 2006a). The rock Clovis has the highest Gt

concentration (A_{Gt} ~37%). The detection of Gt in multiple outcrop rocks implies an extensive occurrence at Husband Hill in particular, and perhaps in the Columbia Hills in general. And second, jarosite ((K,Na,H_3O)(Fe,Al)$_3$(SO_4)$_2$(OH,Cl)$_6$, where Fe > Al and OH > Cl) is present throughout Meridiani Planum in the S-rich outcrop (Burns formation) (Morris *et al.*, 2006b). The jarosite concentration is remarkably constant throughout the Burns formation (A_{Jar} ~29%). Both Gt and Jar yield ~10 wt.% H_2O upon dehydroxylation, so that Clovis and the Burns formation have the equivalent of ~1 to 2 wt.% H_2O based on just their Gt and Jar contents, respectively. On the basis of elemental data and mineralogical compositions constrained by MB data, Clark *et al.* (2005) estimated that the Burns formation might have the equivalent of ~6 to 20 wt.% H_2O overall.

The jarosite detection is also important because its formation is constrained to acid-sulfate environments (pH < 4 at room temperature (*e.g.*, Dutrizac and Jambor, 2000; Stoffregen *et al.*, 2000). Under hydrothermal conditions, jarosite can form at pH = 1 to 2, and hematite instead of goethite is the favored hydrolysis product (Stoffregen *et al.*, 2000). The alteration of a basaltic precursor resulting in the S-rich Burns formation could have occurred under oxidizing, acid-sulfate conditions provided by interactions with acid-sulfate (possibly hydrothermal) waters (Burns, 1988; Burns and Fisher, 1990; McLennan *et al.*, 2005) and/or condensation of SO_2-rich volcanic emanations (Clark and Baird, 1979; Settle, 1979; Banin *et al.*, 1997). Jarosite is a known product of alteration of basaltic/andesitic precursors in association with acid-sulfate volcanic activity on the Earth (*e.g.*, Johnson, 1977; Morris *et al.*, 1996, 2000; Bishop *et al.*, 1998). Interestingly, on Mauna Kea volcano (Hawaii), small Hm-rich spherules are also found in S-rich basaltic material (Morris *et al.*, 2005).

Other evidence based on Fe mineralogical compositions point to aqueous activity. The Independence Class rocks (Independence and Assemblee) have a Fe^{2+} mineral assemblage that is atypical for unaltered igneous rocks ($A_{Ilm} + A_{Chr} > A_{Ol} + A_{Px}$). This result, plus their low Fe_T concentrations (<1.0 moles/24(O+Cl); Figure 6a), suggests dissolution of Ol and Px and subsequent leaching of Fe. The residual rock has an elemental composition that suggests the presence of the phyllosilicate montmorillonite or its compositional equivalent (Clark *et al.*, 2007). The high concentration of Fe^{3+} sulfate in Paso Robles Class soil and its bulk elemental composition point to alteration of basaltic precursors under acid-sulfate and oxidizing conditions. Additional evidence for aqueous alteration in the Columbia Hills is developed in more detail by

Ming *et al.* (2006, 2007; also see Chapter 23), and further details and models for the aqueous alteration history of Meridiani Planum are described by McLennan *et al.* (2005), Grotzinger *et al.* (2005), Squyres *et al.* (2005), Knauth *et al.* (2005), McCollom and Hynek (2005a,b), and Zolotov and Shock (2005). Also see Chapter 24.

8. Mineralogical and oxidation state diversity during isochemical alteration

The Watchtower Class rocks on Husband Hill in the Columbia Hills of Gusev crater are a group of chemically similar but mineralogically diverse outcrop rocks (Squyres *et al.,* 2006; Ming *et al.*, 2006; Morris *et al.*, 2006a). The mineralogical diversity of their Fe-bearing phases is shown in Figure 12. When available, we used APXS and MB analyses for surfaces brushed or ground by the RAT. The values of $A_{Igneous}Fe_T/100$ range from 0.78 moles/24(O+Cl) for Keystone, the least oxidized rock ($Fe^{3+}/Fe_T = 0.43$), to 0.08 moles/24(O+Cl) for Paros, the most oxidized rock at Gusev Crater ($Fe^{3+}/Fe_T = 0.94$). Keystone has ~63% of its iron from primary igneous phases (Px, Ol, Ilm, and Mt) and Paros has only ~6%.

How can such extreme diversity in mineralogical composition and oxidation state be achieved relatively isochemically? However, the presence of goethite in most of the rocks implies aqueous alteration. The nearly constant chemical composition implies low water to rock ratios to prevent or minimize chemical fractionation by transport of elements as dissolved species in aqueous solutions. A terrestrial example of isochemical alteration resulting in mineralogical and oxidation state diversity can be found in the 230 m thick, 55 km diameter melt sheet of the Manicouagan impact structure (Quebec, Canada) (Floran *et al.*, 1976, 1978; Simonds *et al.*, 1978; Morris *et al.*, 1995). There are no statistically significant vertical, horizontal, or radial differences in the regional chemical composition of the melt sheet (Floran *et al.*, 1978), and yet the mineralogical diversity of Manicouagan impact melt rocks is as extreme as for Watchtower Class rocks. Considering just Mössbauer mineralogy (Morris *et al.*, 1995), the values of Fe^{3+}/Fe_T for Manicouagan rocks range from ~0.32 to ~0.92 for rocks whose Fe-bearing phases are dominated by Px and by Hm + npOx, respectively. Oxidative alteration of Manicouagan impact melt rocks is considered to have occurred after the impact event by (hydrothermal) interaction with oxidizing vapors and/or fluids while the rocks were still hot but below solidus temperatures (~915° C) (Floran *et al.*, 1978; Simonds *et al.*, 1978). For example, petrographic studies of Manicouagan and West Clearwater Lake (also in Quebec, Canada)

impact melt rocks show that Hm forms by oxidative (subsolidus) alteration of primary titanomagnetite, mafic minerals, and Fe-bearing glass (Floran *et al.*, 1978; Phinney *et al.*, 1978). In laboratory experiments, Straub *et al.* (1991) produced nanophase Hm as the alteration product of pyroxene under similar oxidative and subsolidus conditions.

Although the Watchtower Class rocks are located in Gusev impact crater, the evidence is equivocal as to whether they are actually a product of target homogenization (by the impact event), crystallization of the impact melt, and subsequent isochemical alteration in a manner analogous to Manicouagan impact melt rocks. The important implication of Manicouagan for alteration processes on Mars is that hydrothermal subsolidus alteration as a regional process can occur isochemically, resulting in the formation of rocks with diverse mineralogical compositions and Fe oxidation states.

An important generalization from Watchtower Class rocks and Manicouagan impact melt rocks is that mineralogical interpretations based solely on chemical data (such as from CIPW normative calculations) are equivocal. Recognizing this, Clark *et al.* (2007) inferred the presence of montmorillonite or its compositional equivalent for an endmember composition derived using chemical mixing models for the highly-altered Independence Class rocks (Independence and Assemblee) in the Columbia Hills. In fact, mini-TES data for the same rocks are not consistent with the presence of phyllosilicates like montmorillonite (Clark *et al.*, 2007). Similarly, Wang *et al.* (2006b) used chemical mixing models to infer the presence of the phyllosilicate kaolinite in the Columbia Hills rock Wooly Patch. In the absence of corroborative mineralogical data, this assignment is also equivocal.

9. Magnetic properties of martian soil and rock

The magnetic properties experiments on the Viking Landers, the Mars Pathfinder rover, and the two MER rovers have shown that martian soil and dust has a strongly magnetic component (*e.g.*, Hargraves *et al.*, 1979; Madsen *et al.*, 1999; Bertelsen *et al.*, 2004; Goetz *et al.*, 2005; also see Chapter 16). Pre-MER estimates for the saturation magnetization of bulk martian soil were 1to 4 Am^2/kg (Morris *et al.*, 2001; Madsen *et al.*, 2003). The Viking and Pathfinder mission teams concluded that the strongly magnetic component was maghemite (γ-Fe_2O_3) produced as a weathering product (*e.g.*, Hargraves *et al.*, 1979; Posey-Dowty *et al.*, 1986; Madsen *et al.*, 1999). Other phases advocated pre-MER as the strongly magnetic component

included (titano)magnetite as a product of igneous activity (Morris *et al.*, 1990, 2001), titanomaghemite as a product of igneous activity and subsequent titanomagnetite oxidation (Coey *et al.*, 1990), and δ-δ'-FeOOH assemblages (Burns, 1980a,b; Towe, 1980) and nanophase hematite (Morris *et al.*, 1989) as products of weathering.

The identification of magnetite in surface rocks and soils by the MER MB instruments firmly establishes that oxide as one and perhaps the dominant strongly magnetic component on the martian surface. The concentration of Fe from magnetite ($A_{Mt}Fe_T/100$) is shown as a function of Fe_T in Figure 13. The horizontal dashed lines are the values of the saturation magnetization (J_s) as a function of Mt concentration using 92 Am^2/kg for bulk magnetite. The samples with the most magnetite are the rocks Peace and Irvine on Husband Hill ($J_s \sim 4$ Am^2/kg). The range of J_s for Laguna Class soil is ~0.4 to 1.2 Am^2/kg, which is at the low end of the range estimated by the magnetic properties experiments.

10. Summary.

The Mössbauer spectrometers on the MER rovers Spirit and Opportunity have provided detailed information on the mineralogical composition and spatial distribution of Fe-bearing phases on opposite sides of Mars at Gusev crater and Meridiani Planum. As of sol 602 at Gusev crater and sol 557 at Meridiani Planum, a total of 12 Fe-bearing phases were identified, and mineralogical assignments were made for 10 of them: olivine, pyroxene, and ilmenite as Fe^{2+}-bearing phases; nanophase ferric oxide, jarosite, hematite, and goethite as Fe^{3+}-bearing phases; magnetite and chromite as Fe^{2+}-and Fe^{3+}-bearing phases; and kamacite as an Fe^0-bearing phase. An octahedrally-coordinatedFe^{3+}-sulfate phase was identified, but a more specific assignment could not be made. Another unidentified oct-Fe^{3+} phase (Fe3D3) appears to be associated with jarosite. These phases occur within four rock supergroups (Weakly Altered Basalt, Altered Low-S Rock, Altered High-S Rock, and Meteorite) and three soil supergroups (Laguna Class soil, Paso Robles Class soil, and Berry Class soil).

The Fe from igneous minerals (olivine, pyroxene, ilmenite, chromite, and magnetite) is primarily associated with Weakly Altered Basalt, which occurs primarily as float and occasionally as outcrop rocks in Gusev crater, and with Laguna Class (basaltic) soil that is ubiquitous at both MER landing sites. Altered Low-S Rock occurs as outcrop and float rocks in the Gusev Columbia Hills. Compared to Weakly Altered Basalt, these rocks have minor to

undetectable Fe from olivine and significant concentrations of Fe from npOx, hematite, and goethite. Altered High-S Rock is the ubiquitous outcrop rock at Meridiani Planum (the Burns formation), with jarosite, hematite, and Fe3D3 the important Fe-bearing phases. Berry Class soil, which is composed of Hm-rich spherules, spherule fragments, and basaltic clasts, occurs at Meridiani Planum primary as lag deposits on ripple crests. Paso Robles Class soil, which has high concentration of an Fe^{3+}-bearing sulfate (not jarosite), occurs as subsurface deposits at isolated locations in the Columbia Hills. It is possible that this soil class is significantly more widespread, but hidden from view by overlying Laguna Class soil except when churned up by rover wheels.

On the basis of MER MB spectra, the strongly magnetic mineral (titano)magnetite is present in Laguna Class soil and in both Weakly Altered Basalt (*e.g.*, Adirondack Class and Irvine Class) and Altered Low-S Rock (*e.g.*, Clovis Class) at Gusev crater. This result is direct mineralogical evidence that the strongly magnetic phase in martian soil and dust is predominantly magnetite formed as a result of igneous processes and not, as generally advocated pre-MER, maghemite (γ-Fe_2O_3) formed during alteration processes.

The Fe mineralogy provides abundant evidence for aqueous alteration on Mars. The most compelling evidence is the identification of two Fe-bearing minerals (jarosite and goethite) that have hydroxide as a part of their crystal structure. Both minerals yield ~10 to 12 wt.% H_2O when dehydroxylated. It is difficult to estimate the regional extent of the goethite occurrence, because there has been no observed spectral signature for the mineral and no associated morphological unit discernable from orbital observations. This situation is not the case for the jarosite-containing Burns formation. On the basis of hematite detections and morphological observations from martian orbit, the Burns formation is laterally extensive (~10^5 km^2; Christensen *et al.*, 2001) with a thickness of ~600 m (Hynek *et al.*, 2002). Jarosite at Meridiani Planum and Fe3Sulfate at Gusev crater are evidence for aqueous processes under acid-sulfate conditions on a planetary scale.

The basaltic bulk chemical composition of the Burns formation and of the highly altered rocks in the Columbia Hills (calculated to a chemical composition with S = Cl = 0) suggests that the alteration occurred at low water-to-rock ratios to prevent or minimize removal of soluble components by leaching (isochemical alteration). The exception to this observation is the Independence Class rocks on Husband Hill, which show evidence of aqueous leaching on the

basis of low Fe concentrations and anomalously high concentrations of ilmenite or chromite. The Wishstone Class rocks are evidence that isochemical alteration can result in mineralogical diversity, implying variable local conditions but still low water-to-rock ratios.

References.

Arvidson, R. E., F. Poulet, R. V. Morris, J.-P. Bibring, J. F. Bell III, S. W. Squyres, P. R. Christensen, G. Bellucci, B. Condet, B. Ehlmann, W. H. Farrand, R. Fergason, J. Griffes, J. Grotzinger, E. A. Guinness, K. E. Herkenhoff, J. R. Johnson, G. Klingelhöfer, Y. Langevin, D. Ming, K. Seelos, R. J. Sullivan, J. G. Ward, S. M. Wiseman, and M. Wolff (2006), Nature and origin of the hematite-bearing plains of Terra Meridiani based on analysis for orbital and Mars Exploration Rover data sets, *J. Geophys. Res*, 111, E12S08, doi:10.1029/2006JE002728.

Arvidson, R. E., S. W. Squyres, R. C. Anderson, J. F. Bell III, J. Brückner, N. A. Cabrol, Calvin.W.M, M. H. Carr, P. R. Christensen, B. C. Clark, L. Crumpler, D. J. Des Marais, C. d'Uston, T. Economou, J. Farmer, W. H. Farrand, W. Folkner, M. Golombek, S. Gorevan, J. A. Grant, R. Greeley, J. Grotzinger, E. Guinness, B. C. Hahn, L. Haskin, K. E. Herkenhoff, J. A. Hurowitz, S. Hviid, J. R. Johnson, G. Klingelhöfer, A. H. Knoll, G. Landis, C. Leff, M. Lemmon, R. Li, M. B. Madsen, M. C. Malin, S. M. McLennan, H. Y. McSween, D. W. Ming, J. Moersch, R. V. Morris, T. Parker, J. W. Rice Jr., L. Richter, R. Rieder, D. S. Rodionov, C. S. Schröder, M. Sims, M. Smith, P. Smith, L. A. Soderblom, R. Sullivan, S. D. Thompson, N. J. Tosca, A. Wang, H. Wänke, J. Ward, T. Wdowiak, M. Wolff, and A. Yen (2006), Overview of the Spirit Mars Exploration Rover Mission to Gusev Crater: Landing Site to the Methuselah Outcrop in the Columbia Hills, *J. Geophys. Res*., *111*, E02S01, doi:10.1029/2005JE002499.

Bancroft, G. M. (1973), *Mössbauer Spectroscopy. An Introduction for Inorganic Chemists and Geochemists*, McGraw Hill, New York.

Banin, A., F. X. Han, I. Kan, and A. Cicelsky (1997), Acidic volatiles and the Mars soil, *J. Geophys. Res.*, *102*, 13341-13356.

Bell III, J. F., H. Y. McSween Jr., J. A. Crisp, R. V. Morris, S. L. Murchie, N. T. Bridges, J. R. Johnson, D. T. Britt, M. P. Golombek, H. J. Moore, A. Ghosh, J. L. Bishop, R. C. Anderson, J. Brucher, T. Economou, J. P. Greenwood, H. P. Gunnlaugsson, R. M. Hargraves, S. Hviid, J. M. Knudsen, M. B. Madsen, R. Reid, R. Rieder, and L. Solderblon (2000), Mineralogic and compositional properties of Martian soil and dust: Results from Mars Pathfinder, *J. Geophys. Res*, *105*, 1721-1755.

Bell III, J. F., S. W. Squyres, R. E. Arvidson, H. M. Arenson, D. Bass, D. Blaney, N. Cabrol, W. Clavin, J. Farmer, W. H. Farrand, W. Goetz, M. Golombek, J. A. Grant, R. Greely, E. Guiness, A. G. Hayes, M. Y. H. Hubbard, K. E. Herkenhoff, M. J. Johnson, J. R. Johnson, J. Joseph, K. M. Kinch, M. T. Lemmon, R. Li, M. B. Madsen, J. N. Maki, M. Malin, E. McCartney, S. McLennan, H. Y. McSween Jr., D. W. Ming, J. E. Moersch, R. V. Morris, E. Z. Noe Dobrea, T. J. Parker, J. Proton, J. W. Rice Jr., F. Seelos, J. Soderblom, L. A. Soderblom, J. N. Sohl-Dickstein, R. J. Sullivan, M.J. Wolff, and A. Wang (2004a), Pancam multispectral imaging results from the Spirit rover at Gusev crater, *Science*, *305*, 800-806.

Bell III, J.F., S.W. Squyres, R.E. Arvidson, H.M. Arneson, D. Bass, W. Calvin, W.H. Farrand, W. Goetz, M. Golombek, R. Greeley, J. Grotzinger, E. Guinness, A.G. Hayes, M.Y.H. Hubbard, K.E. Herkenhoff, M.J. Johnson, J.R. Johnson, J. Joseph, K.M. Kinch, M.T. Lemmon, R. Li, M.B. Madsen, J.N. Maki, M. Malin, E. McCartney, S. McLennan, H.Y. McSween, Jr., D.W. Ming, R.V. Morris, E.Z. Noe Dobrea, T.J. Parker, J. Proton, J.W. Rice,

Jr., F. Seelos, J. Soderblom, L.A. Soderblom, J.N. Sohl-Dickstein, R.J. Sullivan, C. Weitz, M.J. Wolff, Pancam multispectral imaging results from the Opportunity rover at Meridiani Planum, *Science, 306,* 1703-1709, 2004b.

Bell III, J.F., J. Joseph, J.N. Sohl-Dickstein, H.M. Arneson, M.J. Johnson, M.T. Lemmon, and D. Savransky, In-flight calibration and performance of the Mars Exploration Rover Panoramic Camera (Pancam) Instruments, *J. Geophys. Res., 111,* E02S03, doi:10.1029/2005JE002444, 2006.

Bertelsen, P., J.F. Bell III, W. Goetz, H.P. Gunnlaugsson, K.E. Herkenhoff, S.F. Hviid, J.R. Johnson, K.M. Kinch, J.M. Knudsen, M.B. Madsen, E. McCartney, J. Merrison, D.W. Ming, R.V. Morris, M. Olsen, J.B. Proton, M. Sims, S.W. Squyres, A.S. Yen, and the Athena Science Team (2005), Dynamic dust accumulation and dust removal observed on the Mars Exploration Rover Magnets. In *Lunar and Planetary Science XXXVI*, Abstract #2250, Mar. 14-18, 2005, Lunar and Planetary Instutute, Houston, TX (CD-ROM).

Bibring, J.-P., Y. Langevin, J. F. Mustard, F. Poulet, R. E. Arvidson, A. Gendrin, B. Gondet, N. Mangold, P. Pinet, F. Forget, and the OMEGA team (2006), Global mineralogical and aqueous Mars history derived from OMEGA/Mars Express data, *Science*, *312*, 400-404.

Bishop, J. L., H. Froschl, and R. L. Mancinelli (1998), Alteration processes in volcanic soils and identification of exobiologically important weathering products on Mars using remote sensing, *J. Geophys. Res.*, *103*, 31457-31476.

Borggaard, O. K. (1983a), Effect of surface area on mineralogy of iron oxides on their surface charge and anion-adsorption properties, *Clays Clay Minerals*, *31*, 230-232.

Borggaard, O. K. (1983b), The influence of oxides on phosphate adsorption by soil, *J. Soil Sci.*, *34*, 333-341.

Burns, R. G. (1980), Does feroxyhyte occur on the surface of Mars?, *Nature*, *285*, 467.

Burns, R. G. (1980), Feroxyhte on Mars?, *Nature*, *288*, 196.

Burns, R. G. (1988), Gossans on Mars, *Proc. Lunar Planet. Sci. Conf. 18th*, 713-721.

Burns, R. G. (1993), Mossbauer spectral characterization of iron in planetary surface materials, in *Remote Geochemical Analysis: Elemental and Mineralogical Composition*, edited by C. M. Pieters and P. A. J. Englert, pp. 539-556, Cambridge University Press, Cambridge.

Burns, R. G. and D. S. Fisher (1990), Iron-sulfur mineralogy of Mars: Magmatic evolution and chemical weathering products, *J. Geophys. Res.*, *95*, 14,415-14,421.

Burns, R. G. and T. C. Solberg (1990), ^{57}Fe-bearing Oxide, Silicate, and Aluminosilicate Minerals, Crystal Structure Trends in Mössbauer Spectra, in *Spectroscopic Characterization of Minerals and Their Surfaces*, pp. 262-283, American Chemical Society, Washington, D. C.

Christensen, P. R., J. L. Bandfield, R. N. Clark, K. S. Edgett, V. E. Hamilton, T. Hoefen, H. H. Kieffer, R. O. Kuzmin, M. D. Lane, M. C. Malin, R. V. Morris, J. C. Pearl, R. Pearson, T. L. Roush, S. W. Ruff, and M. D. Smith (2000), Detection of crystalline hematite mineralization on Mars by the Thermal Emission Spectrometer, *J. Geophys. Res.*, *105*, 9623-9642.

Christensen, P. R., J. L. Bandfield, V. E. Hamilton, S. W. Ruff, H. H. Kieffer, T. N. Titus, M. C. Malin, R. V. Morris, M. D. Lane, R. L. Clark, B. M. Jakosky, M. T. Mellon, J. C. Pearl, B. J.

Conrath, M. D. Smith, R. T. Clancy, R. O. Kuzmin, T. Roush, G. L. Mehall, N. Gorlick, K. Bender, K. Murray, S. Dason, E. Greene, S. Silverman, and M. Greenfield (2001), Mars Global Surveyor Thermal Emission Spectrometer experiment: Investigation description and surface science results, *J. Geophys. Res.*, *106*, 23,823-23,871.

Christensen, P. R., S. W. Ruff, R. L. Fergason, A. T. Knudson, S. Anwar, R. E. Arvidson, J. L. Bandfield, D. L. Blaney, C. Budney, W. Calvin, T. D. Glotch, M. P. Golombek, N. Gorelick, T. G. Graff, V. E. Hamilton, A. G. Hayes, J. R. Johnson, H. Y. McSween Jr., G. L. Mehall, L. K. Mehall, J. E. Moersch, R. V. Morris, A. D. Rogers, M. D. Smith, S. W. Squyres, M. J. Wolff, and M. B. Wyatt (2004), Initial results from the Mini-TES experiment in Gusev crater from the Spirit rover, *Science*, *305*, 837-842.

Christensen, P. R., M. B. Wyatt, T. D. Glotch, A. D. Rogers, S. Anwar, R. E. Arvidson, J. L. Bandfield, D. L. Blaney, C. Budney, W. M. Calvin, A. Fallacaro, R. L. Fergason, N. Gorelick, T. G. Graff, V. E. Hamilton, A. G. Hayes, J. R. Johnson, A. T. Knudson, H. Y. McSween Jr., L. K. Mehall, J. E. Moersch, R. V. Morris, M. D. Smith, S. W. Squyres, S. W. Ruff, and M. J. Wolff (2004), Mineralogy at Meridiani Planum from the Mini-TES experiment on the Opportunity rover, *Science*, *306*, 1733-1739.

Clark, B. C., R. E. Arvidson, R. Gellert, R. V. Morris, D. W. Ming, L. Richter, S. W. Ruff, J. Michalski, W. Farrand, A. Yen, K. E. Herkenhoff, R. Li, S. W. Squyres, and C. Schröder (2006), Evidence for Montmorillonite or its Compositional Equivalent in the Columbia Hills, Mars , *J. Geophys. Res.*, in press.

Clark, B. C. and A. K. Baird (1979), Is the Martian lithosphere sulfur rich?, *J. Geophys. Res.*, *84*, 8395-8403.

Clark, B. C., R. V. Morris, S. M. McLennan, R. Gellert, B. Jolliff, A. H. Knoll, S. W. Squyres, T. W. Lowenstein, D. W. Ming, N. J. Tosca, A. Yen, P. R. Christensen, S. Gorevan, J. Bruckner, W. Calvin, G. Dreibus, W. Farrand, G. Klingelhöfer, H. Waenke, J. Zipfel, J. F. Bell III, J. Grotzinger, H. Y. McSween, and R. Rieder (2005), Chemistry and mineralogy of outcrops at Meridiani Planum, *Earth. Planet. Sci. Lett.*, *240*, 73-94.

Coey, J. M. D., S. Morup, M. B. Madsen, and J. M. Knudsen (1990), Titanomaghemite in magnetic soils on Earth and Mars, *J. Geophys. Res.*, *95*, 14,423-14,425.

Cornell, R. and U. Schwertmann (1996), *The Iron Oxides: Structure, Properties, Reactions, Occurrences, and Uses*, VHC, New York.

De Grave, E., C. A. Barrero, G. M. Da Costa, R. E. Vandenberghe, and E. Van San (2002), Mössbauer spectra of α- and γ-FeOOH and Fe_2O_3: effects of poor crystallinity and Al-for-Fe substitution, *Clay Minerals*, *37*, 591-606.

De Grave, E., D. Chambaere, and L. H. Bowen (1983), Nature on the Morin transition in Al-substituted hematite, *J. Mag. Mag. Mat.*, *30*, 349-354.

De Grave, E. and A. Van Alboom (1991), Evaluation of ferrous and ferric Mossbauer fractions, *Phys. Chem. Minerals*, *18*, 337-342.

Dutrizac, J. E. and J. L. Jambor (2000), Jarosites and their application in hydrometallurgy, in *Reviews in Mineralogy and Geochemistry, Vol. 40: Sulfate minerals: Crystallography, geochemistry, and environmental significance*, edited by C. N. Alpers, J. L. Jambor, and D. K. Nordstom, pp. 454-479, Mineral. Soc. Amer. & Geochem. Soc., Washington, D. C.

Floran, R. J., R. A. F. Grieve, W. C. Phinney, J. L. Warner, C. H. Simonds, D. P. Blanchard, and M. R. Dence (1978), Manicouagan impact melt, Quebec, 1, Stratigraphy, petrology, and chemistry, *J. Geophys. Res.*, *83*, 2737-2759.

Floran, R. J., C. H. Simonds, R. A. F. Grieve, W. C. Phinney, J. L. Warner, M. J. Rhodes, B. M. Jahn, and M. R. Dence (1976), Petrology, structure and origin of the Manicouagan melt sheet, Quebec, Canada: A preliminary report, *Geophys. Res. Lett.*, *3*, 49-52.

Gellert, R., R. Rieder, R. C. Anderson, J. Brückner, B. C. Clark, G. Dreibus, T. Economou, G. Klingelhöfer, G. W. Lugmair, D. W. Ming, S. W. Squyres, C. d'Uston, H. Wänke, A. Yen, and J. Zipfel (2004), Chemistry of rocks and soils in Gusev crater from the Alpha Particle X-ray Spectrometer, *Science*, *305*, 829-832.

Gellert, R., R. Rieder, J. Brückner, B. C. Clark, G. Dreibus, G. Klingelhöfer, G. Lugmair, D. W. Ming, H. Wänke, A. Yen, J. Zipfel, and S. W. Squyres (2006), Alpha Particle X-Ray Spectrometer (APXS): Results from Gusev crater and calibration report, *J. Geophys. Res.*, *111*, E02S05, 10.1029/2005JE002555.

Goetz, W., P. Bertelsen, C. S. Binau, H. P. Gunnlaugsson, S. F. Hviid, K. M. Kinch, D. E. Madsen, M. B. Madsen, M. Olsen, R. Gellert, G. Klingelhöfer, D. W. Ming, R. V. Morris, R. Rieder, D. S. Rodionov, P. A. de Souza Jr., C. Schröder, S. W. Squyres, T. Wdowiak, and A. Yen (2005), Indication of drier periods on Mars from the chemistry and mineralogy of atmospheric dust, *Nature*, *436/7doi:10.1038/nature03807*.

Golombek, M. P., J. A. Grant, T. J. Parker, D. M. Kass, J. A. Crisp, S. W. Squyres, A. F. C. Haldemann, M. Adler, W. J. Lee, N. T. Bridges, R. E. Arvidson, M. H. Carr, R. L. Kirk, P. C. Knocke, R. B. Roncoli, C. M. Weitz, J. T. Schofield, R. W. Zurek, P. R. Christensen, R. L. Fergason, F. S. Anderson, and J. W. Rice Jr. (2003), Selection of the Mars Exploration Rover landing sites, *J. Geophys. Res.*, *108*, 8072, doi:10.1029/2003JE002074.

Greenwood, N. N. and T. C. Gibb (1971), *Mössbauer Spectroscopy*, Chapman and Hall Ltd, London.

Grotzinger, J. P., R. E. Arvidson, J. F. Bell III, W. Calvin, B. C. Clark, D. A. Fike, M. Golombek, R. Greeley, A. Haldemann, K. E. Herkenhoff, B. L. Jolliff, A. H. Knoll, M. Malin, S. M. McLennan, T. Parker, L. Soderblom, J. N. Sohl-Dickstein, S. W. Squyres, N. J. Tosca, and W. A. Watters (2005), Stratigraphy and sedimentology of a dry to wet eolian depositional system, Burns formation, Meridiani Planum, Mars, *Nature*, *240*, 11-72.

Hargraves, R. B., D. W. Collinson, R. E. Arvidson, and P. M. Cates (1979), Viking magnetic properties experiment: Extended mission results, *J. Geophys. Res.*, *84*, 8379-8384.

Gütlich, P., R. Link, and A. Trautwein (1978), *Mössbauer Spectroscopy and Transition Metal Chemistry*, Inorganic Chemistry Concepts, vol. 3, Springer-Verlag, New York.

Hawthorne, F. C. (1988), Mossbauer Spectroscopy, in *Reviews in Mineralogy,* Volume 18: Spectroscopic Methods in Mineralogy and Geology, edited by F. C. Hawthorne, pp. 255-340, Mineralogical Society of America.

Hynek, B. M., R. E. Arvidson, and R. J. Phillips (2002), Geologic setting and origin of Terra Meridiani hematite deposit, *J. Geophys. Res.*, *107*, 5508, doi:10.1029/2002JE001891.

Johnson, J. H. (1977), Jarosite and akaganeite from White Island volcano, New Zealand: an X-

ray and Mössbauer study, *Geochem. Cosmochem. Acta* , *41*, 539-544.

Klingelhöfer, G., R. V. Morris, B. Bernhardt, C. Schröder, D. S. Rodionov, P. A. de Souza Jr., A. Yen, R. Gellert, E. N. Evlanov, B. Zubkov, J. Foh, U. Bonnes, E. Kankeleit, P. Gütlich, D. W. Ming, F. Renz, T. Wdowiak, S. W. Squyres, and R. E. Arvidson (2004), Jarosite and hematite at Meridiani Planum from Opportunity's Mössbauer spectrometer, *Science, 306*, 1740-1745.

Klingelhöfer, G., E. DeGrave, R. V. Morris, A. Van Alboom, V. G. de Resende, P. A. De Souza, D. Rodionov, C. Schröder, D. W. Ming, and A. Yen (2006), Mössbauer spectroscopy of Mars: goethite in the Columbia Hills at Gusev crater, *Hyperfine Interact*, doi:10.1007/s110751-006-9329-y.

Klingelhöfer, G., R. V. Morris, B. Bernhardt, D. Rodionov, P. A. de Souza Jr., S. W. Squyres, J. Foh, E. Kankeleit, U. Bonnes, R. Gellert, C. Schröder, S. Linkin, E. Evlanov, B. Zubkov, and O. Prilutski (2003), Athena MIMOS II Moessbauer spectrometer investigation, *J. Geophys. Res.*, *108*, 8067, doi:10.1029/2003JE002138.

Knauth, L. P., D. M. Burt, and K. H. Wohletz (2005), Impact origin of sediments at the Opportunity landing site on Mars, *Nature*, *438/22/29*, doi:10.1038/nature04383, 1123-1128.

Lane, M. D., M. D. Dyar, and J. L. Bishop (2004), Spectroscopic evidence for hydrous iron sulfate in the Martian soil, *Geophys. Res. Lett.*, *31*, L19702, doi:10.1029/20-04GL021231.

Madsen, M. B., P. Bertelsen, W. Goetz, C. S. Binau, M. Olsen, F. Folkmann, H. P. Gunnlaugsson, K. M. Kinch, J. M. Knudsen, J. Merrison, P. Nornberg, S. W. Squyres, A. S. Yen, J. D. Rademacher, S. Gorevan, T. Myrick, and P. Bartlett (2003), Magnetic Properties Experiments on the Mars Exploration Rover mission, *J. Geophys. Res.*, *108*, 8069, doi:10.1029/2002JE002029.

Madsen, M. B., S. F. Hviid, H. P. Gunnlaugsson, J. M. Knudsen, W. Goetz, C. T. Pedersen, A. R. Dinesen, C. T. Mogensen, M. Olsen, and R. B. Hargraves (1999), The magnetic properties experiments on Mars Pathfinder, *J. Geophys. Res.*, *104*, 8761-8779.

McCammon, C. (1995), Mössbauer spectroscopy of minerals, in *Mineral Physics and Crystallography: A Handbook of Physical Constants*, edited by T. J. Ahrens, pp. 332-347, American Geophysical Union, Washington DC.

McCollom, T. M. and B. M. Hynek (2005a), A volcanic environment for bedrock diagenesis at Meridiani Planum on Mars, *Nature*, *438/22/29*, doi:10.1038/nature04390, 1129-1131.

McCollom, T. M. and B. M. Hynek (2005b), McCollom & Hynek reply, *Nature*, *433/7*, doi:10.1038/nature05213, E2.

McLennan, S. M., J. F. Bell III, W. M. Calvin, P. R. Christensen, B. C. Clark, P. A. de Souza, J. Farmer, W. H. Farrand, D. A. Fike, R. Gellert, A. Ghosh, T. D. Glotch, J. P. Grotzinger, B. Hahn, K. E. Herkenhoff, J. A. Hurowitz, J. R. Johnson, S. S. Johnson, B. Jolliff, G. Klingelhöfer, A. H. Knoll, Z. Learner, M. C. Malin, H. Y. McSween Jr., J. Pocock, S. W. Ruff, L. A. Soderblom, S. W. Squyres, N. J. Tosca, W. A. Watters, M. B. Wyatt, and A. Yen (2005), Provenance and diagenesis of the evaporite-bearing Burns formation, Meridiani Planum, Mars, *Earth Planet. Sci. Lett.*, *240*, 95-121.

McSween, H. Y., R. E. Arvidson, J. F. Bell III, D. Blaney, N. A. Cabrol, P. R. Christensen, B. C. Clark, J. A. Crisp, L. S. Crumpler, D. J. Des Marais, J. D. Farmer, R. Gellert, A. Ghosh, S. Goevan, T. Graff, J. Grant, L. A. Haskin, K. E. Herkenhoff, J. R. Johnson, B. L. Jolliff, G. Klingelhöfer, A. T. Knudson, S. McLennan, K. A. Milam, J. E. Moersch, R. V. Morris, R. Rieder, S. W. Ruff, P. A. de Souza Jr., S. W. Squyres, H. Wanke, A. Wang, M. B. Wyatt, A. Yen, and J. Zipfel (2004), Basaltic rocks analyzed by the Spirit rover in Gusev Crater, *Science*, *305*, 842-845.

McSween, H. Y., M. B. Wyatt, R. Gellert, J. F. Bell III, R. V. Morris, K. E. Herkenhoff, L. S. Crumpler, K. A. Milam, K. R. Stockstill, L. Tornabene, R. E. Arvidson, P. Bartlett, D. Blaney, N. A. Cabrol, P. R. Christensen, B. C. Clark, J. A. Crisp, D. J. Des Marais, T. Economou, J. D. Farmer, W. Farrand, A. Ghosh, M. Golombek, S. Gorevan, R. Greeley, V. E. Hamilton, J. R. Johnson, B. L. Joliff, G. Klingelhöfer, A. T. Knudson, S. McLennan, D. W. Ming, J. E. Moersch, R. Rieder, S. W. Ruff, C. Schröder, P. A. de Souza Jr., S. W. Squyres, H. Wänke, A. Wang, A. Yen, and J. Zipfel (2006), Characterization and petrologic interpretation of olivine-rich basalts at Gusev Crater, Mars, *J. Geophys. Res.*, *111*, E02S10, doi:10.1029/2005JE002477.

Ming, D. W., D. W. Mittlefehldt, R. V. Morris, D. C. Golden, R. Gellert, A. Yen, B. C. Clark, S. W. Squyres, W. H. Farrand, S. W. Ruff, R. A. Arvidson, G. Klingelhöfer, H. Y. McSween, D. S. Rodionov, C. Schröder, P. A. de Souza, Jr., A. Wang, and the Athena Science Team (2006), Geochemical and mineralogical indicators for aqueous processes in the Columbia Hills of Gusev crater, Mars, *J. Geophys. Res.*, *111*, E02S12, doi:10.1029/2005JE002560.

Morris, R.V., T.G. Graff, T.D. Shelfer, and J.F. Bell III (2001), Effect of palagonitic dust coatings on visible, near-IR and Mossbauer spectra of rocks and minerals: Implications for mineralogical remote sensing of Mars. In *Lunar and Planetary Science XXXII*, Abstract #1912, March 12-16, 2001, Houston TX (CD-ROM).

Morris, R. V., G. Klingelhöfer, B. Bernhardt, C. Schröder, D. S. Rodionov, P. A. de Souza Jr., A. Yen, R. Gellert, E. N. Evalonov, J. Foh, E. Kankeleit, P. Gütlich, D. W. Ming, F. Renz, T. Wdowiak, S. W. Squyres, and R. E. Arvidson (2004), Mössbauer mineralogy on Mars: First results from the *Spirit* landing site in Gusev Crater, *Science*, *305*, 833-836.

Morris, R. V., G. Klingelhöfer, C. Schröder, D. S. Rodionov, A. Yen, D. W. Ming, P. A. de Souza Jr., I. Fleischer, T. Wdowiak, R. Gellert, B. Bernhardt, E. N. Evlanov, B. Zubkov, J. Foh, U. Bonnes, E. Kankeleit, P. Gütlich, F. Renz, S. W. Squyres, and R. E. Arvidson (2006a), Mössbauer mineralogy of rock, soil, and dust at Gusev Crater, Mars: Spirit's journey through weakly altered olivine basalt on the Plains and pervasively altered basalt in the Columbia Hills, *J. Geophys. Res.*, *111*, E02S13, doi:10.1029/2005JE002584.

Morris, R. V., G. Klingelhöfer, C. Schröder, D. S. Rodionov, A. Yen, D. W. Ming, P. A. de Souza Jr., I. Fleischer, T. Wdowiak, R. Gellert, B. Bernhardt, U. Bonnes, B. A. Cohen, E. N. Evlanov, J. Foh, P. Gütlich, E. Kankeleit, T. McCoy, D. W. Mittlefehldt, F. Renz, M. E. Schmidt, B. Zubkov, S. W. Squyres, and R. E. Arvidson (2006b), Mössbauer mineralogy of rock, soil, and dust at Meridiani Planum, Mars: Opportunity's journey across sulfate-rich outcrop, basaltic sand and dust, and hematite lag deposits, *J. Geophys. Res.*, *111*, E12S15, doi:10.1029/2006JE00279.

Morris, R. V., D. W. Ming, T. G. Graff, R. E. Arvidson, J. F. Bell III, S. W. Squyres, S. A.

Mertzman, J. E. Gruener, D. C. Golden, L. Le, and G. A. Robinson (2005), Hematite spherules in basaltic tephra altered under aqueous, acid-sulfate conditions on Mauna Kea volcano, Hawaii: Possible clues for the occurrence of hematite-rich spherules in the Burns formation at Meridiani Planum, Mars, *Earth Planet. Sci. Lett.*, *240*, 168-178.

Morris, R. V., D. G. Agresti, H. V. Lauer Jr., J. A. Newcomb, T. D. Shelfer, and A. V. Murali (1989), Evidence for pigmentary hematite on Mars based on optical magnetic and Mössbauer studies of superparamagnetic (nanocrystalline) hematite, *J. Geophys. Res.*, *94*, 2760-2778.

Morris, R. V., D. C. Golden, J. F. Bell III, H. V. Lauer Jr., and J. B. Adams (1993), Pigmenting agents in Martian soils: Inferences from spectral, Mossbauer, and magnetic properties of nanophase and other iron oxides in Hawaiian palagonitic soil PN-9, *Geochim. Cosmochim. Acta*, *57*, 4597-4609.

Morris, R. V., D. C. Golden, J. F. Bell III, T. D. Shelfer, A. C. Scheinost, N. W. Hinman, G. Furniss, S. A. Mertzman, J. L. Bishop, D. W. Ming, C. C. Allen, and D. T. Britt (2000), Mineralogy, composition, and alteration of Mars Pathfinder rocks and soils: Evidence from multispectral, elemental, and magnetic data on terrestrial analogue, SNC meteorite, and Pathfinder samples, *J. Geophys. Res.*, *105*, 1757-1817.

Morris, R. V., D. C. Golden, J. F. Bell III, and H. V. Lauer Jr. (1995), Hematite, pyroxene, and phyllosilicates on Mars: Implications from oxidized impact melt rocks from Manicouagan Crater, Quebec, Canada, *J. Geophys. Res.*, *100*, 5319-5328.

Morris, R. V., D. C. Golden, D. W. Ming, T. D. Shelfer, L. C. Jorgensen, J. F. Bell III, T. G. Graff, and S. A. Mertzman (2001), Phyllosilicate-poor palagonitic dust form Mauna Kea Volcano (Hawaii): A mineralogical analogue for magnetic martian dust?, *J. Geophys. Res.*, *106*, 5057-5083.

Morris, R. V., J. J. Gooding, H. V. Lauer Jr., and R. B. Singer (1990), Origins of Marslike spectral and magnetic properties of a Hawaiian palagonitic soil, *J. Geophys. Res.*, *95*, 14,427-14,434.

Morris, R. V., D. W. Ming, D. C. Golden, and J. F. Bell III (1996), An occurrence of jarositic tephra on Mauna Kea, Hawaii: Implications for the ferric mineralogy of the Martian surface, in *Mineral Spectroscopy: A Tribute to Roger G. Burns*, edited by M. D. Dyar, C. McCammon, and M. W. Schaefer, pp. 327-336, The Geochemical Society, Special Publication No. 5, Houston.

Myneni, S. C. B. (2000), X-ray and vibrational spectroscopy of sulfate in Earth materials, in *Reviews in Mineralogy and Geochemistry, Vol. 40: Sulfate minerals: Crystallography, geochemistry, and environmental significance*, edited by C. N. Alpers, J. L. Jambor, and D. K. Nordstom, pp. 113-172, Mineral. Soc. Amer. & Geochem. Soc., Washington, D. C.

Phinney, W. C., C. H. Simonds, A. Cochran, and P. E. McGee (1978), West Clearwater, Quebec impact structure, Part II: Petrology, *Proc. Lunar Planet. Sci. Conf. 9th*, 2659-2693.

Posey-Dowty, J., B. Moskowitz, D. Crerar, R. Hargraves, L. Tanenbaum, and E. Dowty (1986), Iron oxide and hydroxide precipitation from ferrous solutions and its relevance to martian surface mineralogy, *Icarus*, *66*, 105-116.

Rieder, R., R. Gellert, R. C. Anderson, J. Breuchner, B. C. Clark, G. Dreibus, T. Economou, G. Klingelhöfer, G. W. Lugmair, D. W. Ming, C. d'Uston, H. Waenke, A. Yen, and J. Zipfel

(2004), Chemistry of rocks and soils at Meridiani Planum from the Alpha Particle X-ray Spectrometer, *Science*, *306*, 1746-1749.

Settle, M. (1979), Formation and deposition of volcanic sulfate aerosols on Mars, *J. Geophys. Res.*, *84*, 8343-8354.

Simonds, C. H., R. J. Floran, P. E. McGee, W. C. Phinney, and J. W. Warner (1978), Petrogenesis of melt rocks, Manicouagan impact structure, Quebec, *J. Geophys. Res.*, *83*, 2773-2788.

Squyres, S. W., O. Aharonson, R. E. Arvidson, J. F. Bell III, P. R. Christensen, B. C. Clark, J. A. Crisp, W. Farrand, T. Glotch, M. P. Golombek, J. Grant, J. Grotzinger, K. E. Herkenhoff, J. R. Johnson, B. L. Jolliff, A. H. Knoll, S. M. McLennan, H. Y. McSween, J. M. Moore, J. W. Rice Jr., and N. Tosca (2005), Bedrock formation at Meridiani Planum, *Nature*, *443/7*, doi:10.1038/nature05212, E1-E2.

Squyres, S. W., R. E. Arvidson, J. F. Bell III, J. Brückner, N. A. Cabrol, W. Calvin, M. H. Carr, P. R. Christensen, B. C. Clark, L. Crumpler, D. J. Des Marais, C. d'Uston, T. Economou, J. Farmer, W. Farrand, W. Folkner, M. Golombek, S. Gorevan, J. A. Grant, R. Greeley, J. Grotzinger, L. Haskin, K. E. Herkenhoff, S. Hviid, J. Johnson, G. Klingelhöfer, A. Knoll, G. Landis, M. Lemmon, R. Li, M. B. Madsen, M. C. Malin, S. M. McLennan, H. Y. McSween, D. W. Ming, J. Moersch, R. V. Morris, T. Parker, J. W. Rice Jr., L. Richter, R. Rieder, M. Sims, M. Smith, P. Smith, L. A. Soderblom, R. Sullivan, H. Wänke, T. Wdowiak, M. Wolff, and A. Yen (2004), The Spirit rover's Athena science investigation at Gusev Crater, Mars, *Science*, *305*, 794-799.

Squyres, S. W., R. E. Arvidson, J. F. Bell III, J. Brückner, N. A. Cabrol, W. Calvin, M. H. Carr, P. R. Christensen, B. C. Clark, L. Crumpler, D. J. Des Marais, C. d'Uston, T. Economou, J. Farmer, W. Farrand, W. Folkner, M. Golombek, S. Gorevan, J. A. Grant, R. Greeley, J. Grotzinger, L. Haskin, K. E. Herkenhoff, S. Hviid, J. Johnson, G. Klingelhöfer, A. Knoll, G. Landis, M. Lemmon, R. Li, M. B. Madsen, M. C. Malin, S. M. McLennan, H. Y. McSween, D. W. Ming, J. Moersch, R. V. Morris, T. Parker, J. W. Rice Jr., L. Richter, R. Rieder, M. Sims, M. Smith, P. Smith, L. A. Soderblom, R. Sullivan, H. Wänke, T. Wdowiak, M. Wolff, and A. Yen (2004), The Opportunity rover's Athena science investigation at Meridiani Planum, Mars, *Science*, *306*, 1698-1703.

Squyres, S. W., R. E. Arvidson, D. L. Blaney, B. C. Clark, L. Crumpler, W. H. Farrand, S. Gorevan, K. E. Herkenhoff, J. Hurowitz, A. Kusack, H. Y. McSween, D. W. Ming, R. V. Morris, S. W. Ruff, A. Wang, and A. Yen (2006), Rocks of the Columbia Hills, *J. Geophys. Res*, *111*, E02S11, doi:10.1029/2005JE002562.

Squyres, S. W., R. E. Arvidson, D. Bollen, J. F. Bell III, J. Brückner, N. A. Cabrol, W. M. Calvin, M. H. Carr, P. R. Christensen, B. C. Clark, L. Crumpler, D. J. Des Marais, C. d'Uston, T. Economou, J. Farmer, W. H. Farrand, W. Folkner, R. Gellert, T. D. Glotch, M. Golombek, S. Gorevan, J. A. Grant, R. Greeley, J. Grotzinger, K. E. Herkenhoff, S. Hviid, J. R. Johnson, G. Klingelhöfer, A. H. Knoll, G. Landis, M. Lemmon, R. Li, M. B. Madsen, M. C. Malin, S. M. McLennan, H. Y. McSween, D. W. Ming, J. Moersch, R. V. Morris, T. Parker, J. W. Rice Jr., L. Richter, R. Rieder, C. Schröder, M. Sims, M. Smith, P. Smith, L. A. Soderblom, R. Sullivan, Tosca, N. J. W. H. , T. Wdowiak, M. Wolff, and A. Yen (2006),

Overview of the Opportunity Mars Exploration Rover Mission to Meridiani Planum: Eagle Crater to Purgatory Ripple , *J. Geophys. Res.*, *111*, E12S12, doi:10.1029/2006JE002771..

Stoffregen, R. E., C. N. Alpers, and J. L. Jambor (2000), Alunite-jarosite crystallography, thermodynamics, and geochemistry, in *Reviews in Mineralogy and Geochemistry, Vol. 40: Sulfate minerals: Crystallography, geochemistry, and environmental significance*, edited by C. N. Alpers, J. L. Jambor, and D. K. Nordstom, pp. 453-480, Mineral. Soc. Amer. & Geochem. Soc., Washington, D. C.

Straub, D. W., R. G. Burns, and S. F. Pratt (1991), Spectral signature of oxidized pyroxenes: Implications to remote sensing of terrestrial planets, *J. Geophys. Res.*, *96*, 18819-18830.

Stevens, J. G., A. M. Khasanov, J. W. Miller, H. Pollak, and Z. Li (1998), *Mössbauer Mineral Handbook*, Biltmore Press, Ashville, NC.

Towe, K. M. (1980), Feroxyhyte on Mars?, *Nature*, *288*, 196.

Wang, A., L. A. Haskin, S. W. Squyres, R. Arvidson, B. L. Jolliff, L. Crumpler, R. Gellert, C. Schröder, K. Herkenhoff, J. Hurowitz, N. J. Tosca, W. H. Farrand, R. Anderson, and A. T. Knudson (2006), Sulfate deposition in subsurface regolith exposed in trenches at the plains traversed by Spirit rover in Gusev crater, Mars, *J. Geophys. Res.*, *111*, E02S17, doi:10.1029/2005JE002513.

Wang, A., R. L. Korotev, B. L. Jolliff, L. A. Haskin, L. Crumpler, W. H. Farrand, K. E. Herkenhoff, P. de Souza Jr., A. G. Kusack, J. A. Hurowitz, and N. J. Tosca (2006), Evidence of phyllosilicates in Wooly Patch, an altered rock encountered at West Spur, Columbia Hills, by the Spirit rover in Gusev crater, Mars., *J. Geophys. Res.*, *111*, E02S16, doi:10.1029/2005JE002516.

Wegener, H. (1966), *Der Mössbauer-Effect und Seine Anwendungen in Physik und Chemie*, 2nd ed., Bibliogr. Inst., Mannheim, Germany.

Wertheim, G. K. (1964), *Mössbauer Effect: Principles and Applications*, Academic, San Diego, CA.

Yen, A. S., R. Gellert, C. Schröder, R. V. Morris, J. F. Bell III, A. T. Knudson, B. C. Clark, D. W. Ming, J. A. Crisp, R. E. Arvidson, D. Blaney, J. Brückner, P. R. Christensen, D. J. DesMarais, P. A. de Souza Jr., T. E. Economou, A. Ghosh, Hahn.B.C, K. E. Herkenhoff, L. A. Haskin, J. A. Hurowitz, B. L. Joliff, J. R. Johnson, M. M. B. Klingelhöfer, S. M. McLennan, H. Y. McSween, L. Richter, R. Rieder, D. Rodionov, L. Soderblom, S. W. Squyres, J. Tosca, A. Wang, M. Wyatt, and J. Zipfel (2005), An Integrated View of the Chemistry and Mineralogy of Martian Soils, *Nature*, *436/7, doi:10.1038/nature03637.*

Yen, A. S., D. W. Mittlefehldt, S. M. McLennan, R. Gellert, J. F. Bell III, H. Y. McSween Jr., D. W. Ming, T. J. McCoy, R. V. Morris, M. Golombek, T. Economou, M. B. Madsen, T. Wdowiak, B. C. Clark, B. L. Jolliff, C. Schröder, J. Brückner, J. Zipfel, and S. W. Squyres (2006), Nickel on Mars: Constraints on meteoritic material at the surface, *J. Geophys. Res*, *111*, E12S11, doi: 10.1029/2006JE002797.

Yen, A. S., B. C. Murray, and G. R. Rossmann (1998), Water content of the Martian soil: Laboratory simulations of reflectance spectra, *J. Geophys. Res.*, *103*, 11,125-11,133.

Zolotov, M. Y. and E. L. Shock (2005), Formation of jarosite-bearing deposits through aqueous oxidation of pyrite at Meridiani Planum, Mars, *Geophys. Res. Lett.*, *32*, L21203, doi:1029-2005GL024253.

Table 1. Average Mössbauer parameters δ and ΔE_Q (210-270 K) for MER doublet spectra

Name	Cation[a]	Assignment	Location[b]	Type	δ[c] (mm/s)	ΔE_Q (mm/s)	N[d]
Fe2D1	oct-Fe^{2+}	Olivine	GC	Rock	1.16±0.02[e]	3.00±0.04[e]	26, 26
Fe2D1	oct-Fe^{2+}	Olivine	GC	Soil	1.15±0.02	2.98±0.03	26, 26
Fe2D1	oct-Fe^{2+}	Olivine	MP	Rock	1.15±0.02	3.01±0.02	1, 1
Fe2D1	oct-Fe^{2+}	Olivine	MP	Soil	1.15±0.02	3.00±0.03	18, 18
Fe2D2	oct-Fe^{2+}	Pyroxene	GC	Rock	1.16±0.02	2.17±0.10	59, 54
Fe2D2	oct-Fe^{2+}	Pyroxene	GC	Soil	1.15±0.02	2.12±0.04	28, 26
Fe2D2	oct-Fe^{2+}	Pyroxene	MP	Rock	1.15±0.02	2.22±0.04	10, 10
Fe2D2	oct-Fe^{2+}	Pyroxene	MP	Soil	1.15±0.02	2.13±0.02	17, 17
Fe2D3	oct-Fe^{2+}	Ilmenite	GC	Rock	1.07±0.02	0.80±0.06	7, 8
Fe2D3	oct-Fe^{2+}	Ilmenite	GC	Soil	1.05±0.02	0.79±0.02	1, 1
Fe2D4	tet-Fe^{2+}	Chromite	GC	Rock	0.92	1.26	n/a[f]
Fe3D1	oct-Fe^{3+}	npOx	GC	Rock	0.37±0.02	0.92±0.09	55, 57
Fe3D1	oct-Fe^{3+}	npOx	GC	Soil	0.38±0.02	0.86±0.06	18, 25
Fe3D1	oct-Fe^{3+}	npOx	MP	Rock	0.34±0.02	0.84±0.17	3, 3
Fe3D1	oct-Fe^{3+}	npOx	MP	Soil	0.38±0.02	0.88±0.03	16, 17
Fe3D2	oct-Fe^{3+}	Fe3Sulfate	GC	Soil	0.43±0.02	0.58±0.05	2, 2
Fe3D3	oct-Fe^{3+}	None	MP	Rock	0.37±0.02	0.62±0.03	46, 46
Fe3D4	oct-Fe^{3+}	Jarosite	MP	Rock	0.37±0.02	1.20±0.02	46, 46
Fe3D5	oct-Fe^{3+}	Chromite	GC	Rock	0.35	0.53	n/a[f]

[a]Oct = octahedral; tet = tetrahedral.
[b]GC = Gusev crater; MP = Meridiani Planum.
[c]δ is measured with respect to metallic Fe foil at the same temperature as the sample.
[d]N = number of analyses used in average calculation for δ and ΔE_Q, respectively.
[e]Uncertainty is the larger of the measurement uncertainty and the standard deviation of the average.
[f]n/a = not applicable. Values of δ and ΔE_Q were constrained to values for chromite during the fitting procedures (Morris *et al.*, 2006a)

Table 2. Average Mössbauer parameters δ, ΔE_Q, and B_{hf} (210-270 K) for MER sextet spectra

Name	Cation[a]	Assignment	Location[b]	Type[b]	δ^c (mm/s)	ΔE_Q (mm/s)	B_{hf} (T)	N[d]
Fe0S1	Fe^0	Kamacite	MP	Rock	0.00 ± 0.02^e	0.00 ± 0.02^e	34.7 ± 0.8^e	2, 2, 2
Fe2.5S1	oct-$Fe^{2.5+}$	Magnetite	GC	Rock	0.64 ± 0.02	0.00 ± 0.02	46.9 ± 0.8	1, 1, 1
Fe3S1	tet-Fe^{3+}	Magnetite	GC	Rock	0.31 ± 0.02	0.06 ± 0.02	50.1 ± 0.8	1, 1, 1
Fe3S2	oct-Fe^{3+}	Hematite	GC	Rock[f]	0.38 ± 0.02	-0.13 ± 0.07	52.2 ± 0.8	27, 31, 31
Fe3S2	oct-Fe^{3+}	Hematite	GC	Rock[g]	0.37 ± 0.02	0.18 ± 0.12	53.3 ± 0.8	12, 13, 13
Fe3S2	oct-Fe^{3+}	Hematite	GC	LC-Soil[h]	0.36 ± 0.02	-0.12 ± 0.05	52.3 ± 0.8	5, 5 ,5
Fe3S2	oct-Fe^{3+}	Hematite	GC	PRC-Soil[f,i]	0.39 ± 0.02	-0.16 ± 0.05	51.3 ± 0.8	1, 1 ,1
Fe3S2	oct-Fe^{3+}	Hematite	GC	PRC-Soil[g,i]	0.36 ± 0.02	0.05 ± 0.02	53.3 ± 0.8	1, 1 ,1
Fe3S2	oct-Fe^{3+}	Hematite	MP	Rock[j]	0.36 ± 0.02	-0.05 ± 0.06	51.9 ± 0.8	41, 41, 41
Fe3S2	oct-Fe^{3+}	Hematite	MP	BC-Soil[k]	0.36 ± 0.02	-0.16 ± 0.05	52.4 ± 0.8	17, 17, 17
Fe3S3	oct-Fe^{3+}	Goethite	GC	Rock	0.38 ± 0.02	-0.17 ± 0.03	35.5 ± 0.8	3, 3, 3

[a]Oct = octahedral; tet = tetrahedral.
[b]GC = Gusev crater; MP = Meridiani Planum.
[c]δ is measured with respect to metallic Fe foil at the same temperature as the sample.
[d]N = number of analyses used in average calculation for δ, ΔE_Q, and B_{hf}, respectively.
[e]Uncertainty is the larger of the measurement uncertainty and the standard deviation of the average.
[f]Average of all sextets with $\Delta E_Q < 0$ mm/s. Includes data from one and two Hm sextet fits. Two Hm sextets are required to fit spectra that contain subspectra from Hm above and below the Morin transition (*e.g.*, PotOfGold at Gusev crater (Morris *et al.*, 2006a).
[g]Average of all sextets with $\Delta E_Q > 0$ mm/s. Includes data from one and two Hm sextet fits.
[h]Laguna class soil.
[i]Paso Robles class soil.
[j]Altered High-S Rock (Burns formation).
[k]Berry Class soil.

Table 3. Average concentration of Fe from individual Fe-bearing phases ($A_xFe_T/100$) in supergroups of Gusev crater and Meridiani Planum rock and soil.

	Gusev Crater						Meridiani Planum					
	Weakly Altered Basalt	Altered Low-S Rock	Altered High-S Rock	Laguna Class Soil	Paso Robles Class Soil	Berry Class Soil	Weakly Altered Basalt	Altered Low-S Rock	Altered High-S Rock	Laguna Class Soil	Paso Robles Class Soil	Berry Class Soil
$\Sigma(A_xFe_T/100) = F_T$; units = moles/24(O+Cl)[a]												
$A_{Ol}Fe_T/100$	0.85±0.34[b]	0.10±0.12	--	0.66±0.10	0.13±0.08	--	0	--	0.03±0.02	0.72±0.14	--	0.62±0.13
$A_{Px}Fe_T/100$	0.74±0.14	0.37±0.21	--	0.63±0.08	0.19±0.06	--	1.78±0.11	--	0.24±0.06	0.83±0.13	--	0.71±0.19
$A_{Ilm}Fe_T/100$	0.00±0.01	0.04±0.06	--	0.01±0.03	0	--	0	--	0	0	--	0
$A_{Chr}Fe_T/100$	0	0.01±0.03	--	0	0	--	0	--	0	0	--	0
$A_{Mt}Fe_T/100$	0.39±0.27	0.15±0.13	--	0.16±0.04	0.11±0.01	--	0	--	0	0.13±0.02	--	0.11±0.11
$A_{npOx}Fe_T/100$	0.23±0.10	0.44±0.19	--	0.41±0.14	0	--	0.01±0.02	--	0.03±0.17	0.43±0.18	--	0.44±0.11
$A_{Fe3Sulfate}Fe_T/100$	0	0	--	0	1.35±0.17	--	0	--	0	0	--	0
$A_{Fe3D3}Fe_T/100$	0	0	--	0	0	--	0	--	0.34±0.04	0	--	0
$A_{Jar}Fe_T/100$	0	0	--	0	0	--	0	--	0.51±0.06	0	--	0
$A_{Hm}Fe_T/100$	0.03±0.03	0.28±0.21	--	0.05±0.04	0.31±0.25	--	0	--	0.63±0.08	0.09±0.04	--	1.62±0.79
$A_{Gt}Fe_T/100$	0	0.18±0.20	--	0	0	--	0	--	0	0	--	0
Fe_T	2.24±0.22	1.56±0.38	--	1.91±0.11	2.07±0.40	--	1.80±0.09	--	1.75±0.10	2.21±0.18	--	3.49±0.60
S^c	0.28±0.15[d]	0.55±0.21	--	0.68±0.24	3.17±0.04	--	0.06±0.01	--	2.27±0.26	0.64±0.11	--	0.61±0.07
Other Parameters												
Fe^{3+}/Fe_T	0.24±0.11	0.63±0.18	--	0.30±0.07	0.83±0.05	--	0.01±0.01	--	0.85±0.03	0.28±0.09	--	0.60±0.13
N^e	15	35	0	24	2	0	3[f]	0	20[g]	10	0	13

[a]MB and APXS data from Morris *et al.* (2006,a,b), Gellert *et al.* (2004), Rieder *et al.* (2004), and Yen *et al.* (2006). Pie diagrams showing distribution of Fe among Fe-bearing phases (values of A_x) are shown in Figure 9.

[b]Average concentration and 1σ standard deviation of the average.

[c]Excludes analyses of undisturbed surfaces when analyses of RAT-brushed or RAT-ground surfaces are available.

[d]Excludes Peace and Alligator, which have a Mg-sulfate cement (Ming *et al.*, 2006) but are Weakly Altered Basalt with respect to Fe-bearing phases.

[e]Number of targets with both MB and APXS data.

[f]All analyses are for Bounce Rock. S concentration is from one analysis of a RAT-ground surface; uncertainty is measurement uncertainty.

[g]Includes only analyses for RAT-ground surfaces.

Table 4. Classification, target name, location, oxidation state (Fe^{3+}/Fe_T), and $A_{Igneous}$ of rocks at Gusev crater and Meridiani Planum.

Rock Name	Class[a]	Subclass[a]	Mössbauer Target Name[b]	Location[c]	Fe^{3+}/Fe_T	$A_{Igneous}$ (%)
Rock Supergroup: Weakly Altered Basalt[d]						
Adirondack	Adirondack	--	A034RR0 (Adirondack_Blue)	GC Pl	0.16[e]	93[f]
Humphrey	Adirondack	--	A060RR0 (Humphrey Heyworth2)	GC Pl	0.15	93
Mazatzal	Adirondack	--	A084RR0 (Mazatzal_Brooklyn)	GC Pl	0.10	95
PaperBack	Adirondack	--	A076RU0 (PaperBack_Appendix)	GC Pl	0.23	80
Route66	Adirondack	--	A100RB (Route66_SoHo)	GC HH	0.07	93
Backstay	Backstay	--	A510RB0 (Backstay_Scuppler)	GC HH	0.23	82
Bounce Rock	Bounce Rock	--	B067RR0 (BounceRock_Case)	MP Pl	0.00	100
Irvine	Irvine	--	A602RU0 (Irvine)	GC HH	0.36	90
Alligator	Peace	--	A385RB0 (Alligator_Jambalaya)	GC HH	0.31	86
Peace	Peace	--	A379RR0 (Peace_Justice2)	GC HH	0.37	86
Joshua	Other Rock	Joshua	A150RU0 (Mohave_Joshua)	GC Pl	0.26	87
MimiShoe	Other Rock	Joshua	A042RU0 (MimiShoe_Lace)	GC Pl	0.43	77
Rock Supergroup: Altered Low-S Rock[d]						
Clovis	Clovis	Clovis	A218RR0 (Clovis_Plano)	GC WS	0.84	17
Ebenezer	Clovis	Clovis	A233RR0 (Ebenzer_Ratchit2)	GC WS	0.83	31
Lutefisk	Clovis	Clovis	A303RB0 (Lutefisk_Roe)	GC WS	0.65	49
Temples	Clovis	Clovis	A269RU (Temples_Dwarf)	GC WS	0.74	33
Tetl	Clovis	Clovis	A275RU0 (Tetle_Clump)	GC WS	0.70	47
Uchben	Clovis	Clovis	A288RR0 (Uchben_Koolik)	GC WS	0.79	31
Wooly Patch	Clovis	Wooly Patch	A200RR0 (WoolyPatch_Mastadon)	GC WS	0.61	50
Assemblee	Independence	--	A568RU0 (Assemblee_Gruyere)	GC HH	0.37	91
Independence	Independence	--	A542RS0 (Independence_Penn2)	GC HH	0.25	32
BreadBox	Other Rock	PotOfGold	A176RU0 (Breadbox_Sourdough)	GC WS	0.47	58
Fork Knox	Other Rock	PotOfGold	A166RU0 (FortKnox_Goldbar)	GC WS	0.52	49
Keel Davis	Watchtower	Keel	A486RB0 (Keel_Davis)	GC HH	0.73	25
Keel Reef	Watchtower	Keel	A483RU0 (Keel_Reef)	GC HH	0.64	43
Keystone	Watchtower	Keystone	A472RB0 (Keystone_Haunch)	GC HH	0.43	57
Paros	Watchtower	Watchtower	A493RB0 (LarrysLookout_Paros)	GC HH	0.94	4
Pequod	Watchtower	Watchtower	A498RU0 (Pequod_Ahab)	GC HH	0.88	6
Watchtower	Watchtower	Watchtower	A418RR0 (WatchTower_Joker)	GC HH	0.83	14
Champagne	Wishstone	--	A358RR0 (Champagne_RAT2)	GC HH	0.45	56
WishingWell	Wishstone	--	A350RU0 (WishingWell_Dreaming)	GC HH	0.41	63
Wishstone	Wishstone	--	A336RR0 (Wishstone_Chisel)	GC HH	0.40	62
PotOfGold	Other Rock	PotOfGold	A173RR0 (HanksHollow_PotOfGold)	GC WS	0.62	39
StringOfPearls	Other Rock	PotOfGold	A178RU (StringOfPearls_Pearl)	GC WS	0.43	59
Rock Supergroup: Altered High-S Rock[g]						
Blackcow	Burns Outcrop	--	B308RR0 (Blackcow_Wharenhui)	MP-End	0.81	19
Bylot	Burns Outcrop	--	B196RR0 (Bylot_Aktineq3)	MP-End	0.85	15
Diamond Jenness	Burns Outcrop	--	B179RR0 (DiamondJenness_Holeman3)	MP-End	0.88	12
Escher	Burns Outcrop	--	B219RR0 (Escher Kirchner)	MP-End	0.84	16
Flatrock	Burns Outcrop	--	B045RR0 (FlatRock_Mojo2)	MP Eag	0.85	25
Guadalupe	Burns Outcrop	--	B035RR0 (Guadalupe_King3)	MP Eag	0.90	10
IceCream	Burns Outcrop	--	B548RR0 (IceCream_Onescoop)	MP Pl	0.87	13
Inuvik	Burns Outcrop	--	B188RR0 (Inuvik_Tuktoyaktuk)	MP-End	0.84	16
Lionstone	Burns Outcrop	--	B108RR0 (LionStone_NummaNewNormal)	MP-End	0.86	14
Kentucky	Burns Outcrop	--	B144RR0 (Kentucky_CobbleHill)	MP-End	0.84	16

Table 4. Continued

Rock Name	Class	Subclass	Mössbauer Target Name	Location	Fe^{3+}/Fe_T	$A_{Igneous}$
Mackenzie	Burns Outcrop	--	B183RR0 (Mackenzie_Campbell2)	MP-End	0.84	16
Manitoba	Burns Outcrop	--	B152RR0 (Manitoba_Grindstone)	MP-End	0.82	19
McKittrick	Burns Outcrop	--	B032RR0 (McKittrick_MiddleRAT_	MP Eag	0.87	13
Millstone	Burns Outcrop	--	B163RR0 (Millstone_Drammensfjord)	MP-End	0.78	22
Ontario	Burns Outcrop	--	B150RR0 (Ontario London)	MP-End	0.81	19
Pilbara	Burns Outcrop	--	B088RR0 (Pilbara_Golf)	MP-Frm	0.90	10
Tennessee	Burns Outcrop	--	B1400RR (Tennessee_Vols)	MP-End	0.85	15
Virginia	Burns Outcrop	--	B148RR0 (LayerC_Virginia)	MP-End	0.82	18
Yuri	Burns Outcrop	--	B404RR0 (Yuri_Gagarin)	MP Pl	0.92	8
			Rock Supergroup: Meteorite[d]			
Barberton	Meteorite	--	B121RU0 (FigTree_Barberton2)	MP End	0.06	83
Heat Shield Rock	Meteorite	--	B351RB0 (SpongeBob_Squidward)	MP Pl	0.06	0

[a]Rock classes Gusev crater from Squyres *et al.* (2006), except for Independence Class. Rock subclass from for Gusev crater from Morris *et al.* (2006a).

[b]Target naming convention: Mwwwxyz (Feature-name_Target-name). M =A for MER-A (Gusev Crater) or B for MER-B (Meridiani Planum); www = sol number that data product was returned to Earth. For integrations covering multiple sols, the sol of the first returned data product is used. x = R (rock) or S (soil); y = U (undisturbed), D (disturbed), T (trench), B (RAT-brushed surface), R (RAT-ground surface), S (scuff of rock surface by rover wheel), or G (RAT grindings); z = 0 by default; z = 1, 2, 3… for multiple analyses of the same target on the same sol. For MxxxSTz, z = 1, 2, 3… with increasing number corresponding to increasing depth. Alphanumeric strings before parentheses are unique target identifiers.

[c]GC = Gusev crater; Pl = Plains; WS = West Spur; HH = Husband Hill; MP = Meridiani Planum; Eag = Eagle Crater; End = Endurance Crater.

[d]Includes only the first target for a rock in the order RAT-grind (RR), RAT-brushed (RB), and undisturbed (RU)

[e]Uncertainty = ±0.03.

[f]$A_{Igneous} = A_{Ol} + A_{Px} + A_{Ilm} + A_{Chr} + A_{Mt}$. Note that $A_{Igneous} = (1.0 - MAI)$, where MAI = Mineralogical Alteration Index (Morris *et al.*, 2006a).

[g]Includes only targets of Burns Outcrop exposed by RAT-grinding.

Table 5. Classification, target name, location, oxidation state (Fe^{3+}/Fe_T), and $A_{Igneous}$ of soils at Gusev crater and Meridiani Planum.

Soil Name	Subclass[a]	Mössbauer Target Name[b]	Location[c]	Fe^{3+}/Fe_T	$A_{Igneous}$ (%)
Soil Supergroup: Laguna Class Soil[a]					
Auk	Panda	B237SB0 (Auk_AukRAT)	MP End	0.20[d]	84[e]
BearPaw Panda	Panda	A073SD0 (BearPaw_Panda)	GC Pl	0.25	84
Big Hole May Fly	Boroughs	A113ST1 (BigHole_MayFly)	GC Pl	0.26	82
Big Hole RS2	Boroughs	A114ST2 (Bighole_RS2)	GC Pl	0.44	62
Brians Choice	Liberty	B056SU0 (BlackForest_BriansChoice)	MP Eag	0.27	78
Coffee	Liberty	A281SD0 (TakeABreak_Coffee)	GC WS	0.31	78
Cookie Cutter	Gobi	A182SU0 (CookieCutter_Shortbread)	GC WS	0.38	71
Conjunction	Gobi	A260SD0(Conjunction_Disturbance)	GC WS	0.31	75
Crumble	Panda	A459SU0 (Crumble_Almonds)	GC HH	0.21	84
Cutthroat	Gobi	A122SD0 (Cutthroat_Owens)	GC Pl	0.34	75
Dahlia	Panda	B165SU0 (Millstone_Dahlia)	MP End	0.20	83
Desert Gobi	Gobi	A069SU0 (Desert_Gobi)	GC Pl	0.36	70
FineSoil	Panda	B038SU0 (FineSoil_Paydirt)	MP Eag	0.22	83
First Soil	Gobi	A014SU0 (FirstSoil)	GC Pl	0.29	75
Goldfinger	Panda	A167SU0 (Goldfinger_Jaws)	GC WS	0.26	82
Hells Kitchen	Boroughs	A141ST2 (Boroughs_HellsKitchen)	GC Pl	0.42	65
Hema Trench Bottom	Gobi	B025ST2 (BigDig HemaTrench1)	MP Eag	0.48	55
Hema Trench Wall	Gobi	B026ST1 (BigDig_HemaTrenchWall2)	MP Eag	0.32	72
Jeffs Choice	Liberty	B078ST1 (DogPark_JeffsChoice)	MP Pl	0.27	78
Laguna Hollow Floor	Panda	A049ST2 (LagunaHollow_Floor3)	GC Pl	0.23	84
Laguna Hollow Trout	Liberty	A047SU0 (LagunaHollow_Trout1)	GC Pl	0.30	76
Laguna Hollow Wall	Panda	A050ST1 (LagunaHollow_WallMIonly)	GC Pl	0.23	83
Left of Peanut	Liberty	B367ST1 (TrenchSite_LeftOfPeanut)	MP Pl	0.27	77
Les Hauches	Gobi	B060SU0 (MontBlanc_LesHauches)	MP Eag	0.39	65
Liberty	Liberty	A479SU0 (Liberty_Bell)	GC HH	0.25	79
McDonnell	Liberty	B123SU0 (HillTop_McDonnell)	MP End	0.28	77
Mazatzal Flats	Liberty	A077SU0 (MazatzalFlats_Soil1)	GC Pl	0.30	79
Meringue	Liberty	B055SU0 (Meringue_MBone)	MP Eag	0.24	80
Merlot	Panda	B011SU0 (Merlot_Tarmac)	MP Eag	0.22	82
Mill Basin	Boroughs	A140ST1 (Boroughs_MillBasin)	GC Pl	0.36	69
Mimi Tracks	Panda	A043SD0 (MimiTracks_Middle)	GC Pl	0.27	78
Mount Hillyer	Liberty	A135SD0 (MountHillyer_HorseFlats)	GC Pl	0.26	80
Paso Dark	Liberty	A426SD0 (PasoRobles2_PasoDark)	GC HH	0.27	80
Penny	Panda	A342SD0 (Penny_DS1)	GC HH	0.22	84
Rocknest	Panda	B246SU0 (Rocknest_VoidMod)	MP End	0.21	84
Scruffy	Panda	B373SD0 (Trench_Scruffy)	MP Pl	0.21	83
Shreaded	Panda	A158SD0 (Shreaded_Dark4)	GC WS	0.22	83
Waffel Flats	Gobi	A110SU0 (WaffelFlats_Soil1)	GC Pl	0.40	75
Yams	Liberty	A316SD0 (Yams_Turkey)	GC WS	0.30	76
Soil Supergroup: Paso Robles Class					
Paso Light	--	A429SD0 (PasoRobles2_PasoLight1)	GC HH	0.79	24
Paso Robles	--	A401SD0 (Pasadena_PasoRobles)	GC HH	0.86	17

Table 5. Continued

Soil Name	Subclass	Mössbauer Target Name	Location	Fe^{3+}/Fe_T	$A_{Igneous}$ (%)
Soil Supergroup: Berry Class					
Aegean Crest	Moessberry	B073SU0 (Seas_AegeanCrest)	MP Pl	0.76	30
Berry Stop	Moessberry	B097SU0 (BerryStop_LeahsChoice)	MP Pl	0.63	40
Berry Survey	Moessberry	B222SU0 (BerrySurvey_Cluster3)	MP End	0.64	37
Cavair	Nougat	B369SU0 (TrenchRipple_Cavair_Tweaked)	MP Pl	0.45	60
Cleo	Moessberry	B063SU0 (Whitestreak_Cleo3)	MP Pl	0.67	36
Freckles	Nougat	B017SU (BerryFlats_Freckles)	MP Eag	0.46	54
Fred Ripple	Moessberry	B091RU0 (PhotoTIDD_FredRipple)	MP Pl	0.66	39
Hematite Slope	Nougat	B023SU0 (HematiteSlope_Hema2)	MP Eag	0.39	65
Jack Russell	Moessberry	B080SU0 (DogPark_Jack Russell)	MP Pl	0.64	36
Mayberooz	Moessberry	B420SU0 (Ripple Mayberooz)	MP Pl	0.66	34
Mobarak	Moessberry	B415SU0 (MattsChoice_Mobarak)	MP Pl	0.61	40
MoessBerry	Moessberry	B048SU0 (BerryBowl_MoessBerry)	MP Eag	0.79	21
Mud Pie	Nougat	B054SU0 (MudPie_Coconut2)	MP Eag	0.30	75
Munter	Nougat	B062SU0 (BlackPatch Munter)	MP Pl	0.40	66
Norooz	Moessberry	B419SU0 (Ripple_Norooz)	MP Pl	0.65	35
Nougat	Nougat	B090SD0 (PhotoTIDD_Nougat)	MP Pl	0.40	65
Nullarbor	Moessberry	B084SU0 (Nullarbor_GreatSandy)	MP Pl	0.70	33
Panaluu	Moessberry	B052SU (Goal5WorkVolume_Panaluu)	MP Eag	0.78	28
Purgatory	Nougat	B509SD0 (Purgatory_Track2)	MP Pl	0.49	55
Recovery Soil	Moessberry	B445SU0 (RecoverySoil_Cure)	MP Pl	0.63	39
Ripple Crest	Moessberry	B368SU0 (TrenchRipple_RippleCrest2b)	MP Pl	0.75	25
Vanilla	Nougat	B053SU0 (Goal3Field_Vanilla)	MP Eag	0.35	70
Unclassified Soil					
Doubloon	Doubloon	A502SU0 (Pequod_Doubloon)	GC HH	0.38	66

[a]Soil classes and subclasses from Morris *et al.* (2006a,b).

[b]See Table 4 footnote for target naming convention.

[c]GC = Gusev crater; Pl = Plains; WS = West Spur; HH = Husband Hill; MP = Meridiani Planum; Eag = Eagle Crater; End = Endurance Crater.

[d]Uncertainty = ±0.03.

[e]$A_{Igneous} = A_{Ol} + A_{Px} + A_{Ilm} + A_{Chr} + A_{Mt}$. Note that $A_{Igneous} = (1.0 - MAI)$, where MAI = Mineralogical Alteration Index (Morris *et al.*, 2006a).

Figure Captions.

Figure 1. Energy level diagrams for ^{57}Fe for the cases of singlet, doublet, and sextet transmission Mössbauer spectra, schematic representation of the corresponding MB spectra and equations used for calculation of MB parameters δ, ΔE_Q, and B_{hf}, and representative geologic materials. MER MB spectra are measured in backscatter geometry, so the MB spectra are emission peaks (*i.e.*, essentially the inverse of the typical laboratory transmission geometry spectra shown here). For MER instruments (Klingelhöfer *et al.*, 2003), δ is measured with respect to the center point of the spectrum of metallic Fe foil at approximately the same temperature as the sample. For peak centers in units of mm/s and B_{hf} in units of tesla (T), the constant in the formula $B_{hf} = $ (constant)(v6-v1) equals 3.101.

Figure 2. Images for the MIMOS II Mössbauer spectrometer and selected surface targets for MB analysis at Gusev crater and Meridiani Planum. Image identifications are given in the figure. Pancam images were downloaded from http://pancam.astro.cornell.edu/ (Bell *et al*., 2006) **(a)** Approximate true color image of Spirit's Instrument Deployment Device (IDD) showing the sensor head of the MIMOS II Mössbauer spectrometer. The hole in the contact plate (1.5 cm diameter) defines the field of view for the instrument. The contact plate has a temperature sensor for measurement of martian surface temperatures. Note the small patch of soil adhering to the contact plate. **(b)** Approximate true color image showing hole ground by the RAT in Burns Outcrop Class rock McKittrick. The hole diameter is ~4 cm. MB spectra from the hole are shown in Figures 4h and 4i. **(c)** Approximate true color image showing the RAT brush "mosaic" on the Adirondack class rock Route66 at Gusev crater. MB spectrum is shown in Figure 4a. **(d)** Approximate true color image showing spherules in the "Blueberry Bowl" at Eagle crater, Meridiani Planum. MB spectra were obtained from a spherule-free region of the outcrop rock and from the spherules that collected in the bowl (sample B048SU0 (BerryBowl_MoessBerry) in Figure 4l). **(e)** Approximate true color image showing a RAT brush mosaic and a RAT hole in the Clovis Class rock Clovis (samples A213RU0, A215RB0, and A218RR (Clovis_Plano) in Figure 4k) at West Spur in Gusev crater. **(f)** False color image showing trench dug with rover wheels through a ripple on the plains at Meridiani Planum south of Endurance crater. MB spectra were obtained for soils at the ripple crest (Berry Class soil; similar to sample A415SU0

(MattsRipple_Mobarak) in Figure 4m), ripple trough (Berry Class soil), and trench bottom (Laguna Class soil). Note that the contact plate creates a "noseprint" in soft soil. (**g**) Approximate true color image showing a trench dug with rover wheels on the northwestern flank of Husband Hill. As shown by the noseprints, MB spectra were obtained on the "white" soil (Paso Robles Class soil) and on the "dark" soil (Laguna Class soil). The white soil MB spectrum is similar to sample A401SD0 (Pasadena_PasoRobles) in Figure 4g. (**h**) Microscopic Imager (MI) image showing MB noseprint for sample B060SU0 (MontBlanc_LesHauches) in the fine-grained deposit of dust just below the downwind lip of Eagle crater. The spectrum is similar to sample A069SU0 (Desert_Gobi) in Figure 4e.

Figure 3. Fe-bearing phase identification diagrams for doublet (**a** and **c**) and sextet (**b** and **d**) spectra acquired at Gusev crater (GC) and Meridiani Planum (MP). Generic names have the form FeXYZ where X = Fe oxidation state, Y = D (doublet) or S (sextet), and Z = a sequence number for phases with the same values of X and Y. Phase assignments are given in parentheses (Ol = olivine, Px = pyroxene, Ilm = ilmenite; Chr = chromite; npOx = nanophase ferric oxide; Fe3Sulfate = ferric sulfate; Jar = jarosite; Mt = magnetite; Hm = hematite; Gt = goethite; Kam = kamacite). Chr has two doublets (Fe2D4 and Fe3D5), and Mt has two sextets (Fe2.5S1 and Fe3S1). One Fe-bearing phase (Fe3D3) was not assigned a mineralogical composition. The large range in values of ΔE_Q for Hm results from a magnetic transition (the Morin transition at ~260 K for pure, well-crystalline bulk hematite) that occurs within the martian diurnal temperature range (~180 to300 K). The isomer shift (δ) is measured with respect to the center point of the spectrum of metallic Fe foil at nominally the same temperature as the sample temperature.

Figure 4. Mössbauer spectra from the MER MIMOS II instruments that have high proportions of Fe from each of the 14 identified MB doublets and sextets: (**a**) Fe2D1 (Ol) in Adirondack class rock Route66; (**b**) Fe2D2 (Px) in rock Irvine; (**c**) Fe2D3 (Ilm) in Wishstone class rock Wishstone; (**d**) Fe2D4 and Fe3D5 (Chr) in Independence class rock Assemblee; (**e**) Fe3D1 (npOx) in Laguna class undisturbed soil sample Desert_Gobi; (**f**) Fe3D1 (npOx) in Watchtower Class rock LarrysLookout; (**g**) Fe3D2 (Fe3Sulfate) in Paso Robles Class soil sample Pasadena_PasoRobles; (**h**) Fe3D3 (unassigned) and Fe3D4 (Jar) in Burns Outcrop Class; (**i**) same as (**h**) except MB spectrum was acquired over a narrow velocity range; (**j**) Fe2.5S1 and

Fe3S1 (Mt) in Peace Class rock Peace; (**k**) Fe3S3 (Gt) in Clovis Blass rock Clovis; (**l**) Fe3S2 (Hm) in Berry Class undisturbed soil sample BerryBowl_Moessberry; (**m**) Fe3S2 (Hm) in Berry Class undisturbed soil sample MattsRipple_Mobarak; and (**n**) Fe0S1 (Kam) in Heat Shield Rock. All MB spectra are the sum of spectra for temperatures between 200 and 270 K. Sample naming convention is Uwwwxyz, where U = A for Gusev crater or U = B for Meridiani Planum, www = sol number, x = R (rock) or S(soil), y = U (undisturbed), D (disturbed), B (RAT brush), or R (RAT grind), and z = 0, 1, 2, … as appropriate to keep sample names unique (usually, z = 0). The y-axis is TC/BC – 1.0, where TC = total counts and BC = baseline counts. The maximum value of TC/BC – 1.0 for each spectrum is given in the figure as $(TC/BC – 1.0)_{MAX}$.

Figure 5. Histograms for number of MB analyses having >10% Fe from each of the 12 Fe-bearing phases for rocks (**a** and **c**) and soils (**b** and **d**) at Gusev crater (**a** and **b**) and Meridiani Planum (**c** and **d**). The numbers above each non-zero column refer to the number of MB analyses where the Fe percentage from an Fe-bearing phase is >10% (upper) and the total number of MB analyses where the Fe percentage from an Fe-bearing phase is >0% (lower).

Figure 6. Diagrams for assignment of MER non-meteorite rock samples to supergroups (Weakly Altered Basalt, Altered Low-S Rock, and Altered High-S Rock). (**a**). Fe_T versus $A_{Igneous}Fe_T/100$, where $A_{Igneous} = A_{Ol} + A_{Px} + A_{Ilm} + A_{Chr} + A_{Mt}$. Weakly Altered Basalts are distinguished from altered rocks by high values of Fe_T and $Fe_T \sim A_{Igneous}Fe_T/100$ (dashed line with labeled "y = x"). Independence Class rocks (Ind. Class), having $Fe_T \sim A_{Igneous}Fe_T/100$ and low Fe_T, are Altered Low-S Rocks. (**b**). Fe_T versus $(A_{Jar} + A_{Fe3D3} + A_{Hm})Fe_T/100$. Altered High-S Rocks are distinguished from Altered Low-S Rocks, because Jar, Fe3D3, and Hm are the dominant Fe-bearing phases in the former but not in the latter (**c**). S versus $(A_{Jar} + A_{Fe3D3} + A_{Hm})Fe_T/100$. Altered High-S Rocks have S concentration greater than ~1.5 moles/24(O+Cl) (equivalently, ~14.2 wt.% SO_3). Outcrop surfaces not exposed by grinding with the RAT (open square symbols) tend to have low concentrations of S because the analysis volumes include contributions from soil and dust coatings that have low-S concentrations. (**d**) Fe_T versus $A_{Hm}Fe_T/100$. High concentrations of Fe from Hm are found in rocks from both Gusev crater and Meridiani Planum.

Figure 7. Diagrams for assignment of MER soil samples to supergroups (Laguna Class soil, Paso Robles Class soil, and Berry Class soil). (**a**). Fe_T versus $A_{Igneous}Fe_T/100$. Soils form into Laguna Class (LC), Paso Robles Class (PRC) and Berry Class (BC) supergroups, except for two BC soils that have LC affinities. (**b**). Fe_T versus $(A_{Jar} + A_{Fe3D3} + A_{Hm})Fe_T/100$. BC soils are distinguished from LC soils. (**c**). S versus $(A_{Jar} + A_{Fe3D3} + A_{Hm})Fe_T/100$. The three soil supergroups form into different regions. LC and BC supergroups have S concentrations within the range for Altered Low-S Rock (Figure 6c). PRC soils at Gusev crater have the highest S concentrations measured on Mars. (**d**) Fe_T versus $A_{Hm}Fe_T/100$. Soils do not have detectable concentrations of Jar and Fe3D3 (compare with (**b**)).

Figure 8. Plots of $A_{Igneous}Fe_T/100$ versus $A_{Alteration}Fe_T/100$ for (**a**) rock and (**b**) soil at Gusev crater (GC) and Meridiani Planum (MP). Solid lines correspond to $Fe_T = 2.24$ and 1.80 moles/24(O+Cl). Weakly Altered Basalts (Wk. Alt. Basalt) plot near the upper left corner of (**a**). Assuming that all unaltered martian rocks have $Fe_T > 1.0$ moles/24(O+Cl) and $A_{Alteration}Fe_T/100$ ~ 0 moles/24(O+Cl), compositions that plot on the y-axis of (**a**) with $Fe_T < 1.0$ moles/24(O+Cl) are rocks altered in an open system without retention of Fe-bearing alteration products. Independent Class (Ind. Class) rocks, for example, are examples of rocks that show evidence for alteration in an open system. Samples that plot along a line of constant Fe_T (*e.g.*, $Fe_T = 2.24$ and 1.80 moles/24(O+Cl)) are only potentially related by isochemical alteration (on an H_2O-free basis), because all elemental concentrations must be considered to validate isochemical alteration. For example, in (**a**), Bounce Rock (BR) and MP S-rich outcrop rocks plot along the line with $Fe_T = 1.80$ moles/24(O+Cl) but are not related by isochemical alteration because of differences in major element chemistry (*e.g.*, Rieder *et al.*, 2004).

Figure 9. Pie diagrams showing the average values (1σ standard deviation in parenthesis) of Fe from Fe-bearing phases (A_x, where x = Ol, Px, Ilm, Chr, Mt, npOx, Fe3Sulfate, Fe3D3, Jar, Hm, and Gt) for rock and soil supergroups at Gusev crater (as of sol 602) and Meridiani Planum (as of sol 557): (**a**) Weakly Altered Basalt, (**b**) Altered Low-S Rock, and (**c**) Altered High-S Rock for RAT-ground surfaces, (**d**) Laguna Class soil, (**e**) Paso Robles Class soil, and (**f**) Berry Class soil. Altered High-S Rock and Berry Class soil are not present at Gusev crater and Altered Low-S Rock and Paso Robles Class soil are not present at Meridiani Planum. The distribution of Fe

from Fe-bearing phases for Gusev crater Weakly Altered Basalt (**a**) is very similar to that for Laguna Class soil (**e**), except the latter has more Fe from npOx. The meteorite supergroup (not shown), whose distinguishing characteristic is kamacite as an Fe-bearing phase, includes two rocks from Meridiani Planum (Heat Shield and Barberton) and no rocks from Gusev crater. The average concentrations of Fe associated with iron bearing phases ($A_xFe_T/100$) are given in Table 3.

Figure 10. Supergroup membership of rock and soil analyses and Fe^{3+}/Fe_T as a function of sol number for Gusev crater (**a** and **c**) and Meridiani Planum (**b** and **d**). Sol number is used a proxy for location, and general location names are shown in the figures. The Weakly Altered Basalts are Adirondack (Ad), Mimi Shoe (MS), Humphrey (Hu), Mazatzal (Mz), Route66 (R66), Joshua (Jo), Peace (Pe), Alligator (Al), Backstay (Bs), Irvine (Ir), and Bounce Rock (BR). The significant range in Fe^{3+}/Fe_T for Weakly Altered Basalt results from variable contributions from magnetite which has $Fe^{3+}/Fe_T = 0.67$ for the stoichiometric composition (Fe_3O_4). The Altered Low-S Rocks are Wooly Patch (WP), Clovis (Cl), Ebenezer (Eb), Wishstone (Ws), Champagne (Ch), Watchtower (Wt), Pharos (Ph), Pequod (Pq), Independence (In), and Assemblee (As). Barberton (Bt) and Heat Shield (HS) rocks are meteorites at Meridiani Planum.

Figure 11. Molar concentrations of (**a**) S and (**b**) Cl versus the molar concentration of Fe from npOx ($A_{npOx}Fe_T/100$) for Laguna and Berry class soils and two analyses of thick dust coatings on the Gusev crater rock Mazatzal. The solid lines are linear least squares fits, excluding the subsurface Boroughs trench (Bo Trench) samples in (**a**). The slopes of the lines are upper limits for the molar ratios of S/Fe (0.62) and Cl/Fe (0.12) for npOx (see text). Specific soil samples labeled on the graph are Crumble_Almond (CA), BearPaw Panda (BP), Desert_Gobi (DG), Boroughs_MillBasin and Boroughs_HellsKitchen (Bo), MontBlanc_LesHauches (ML), Lambert_Whymper (LW), BigHole_RS2 (RS2), Purgatory_Track2 (PT), and BigDig_HemaTrench1 (BH).

Figure 12. Pie diagrams showing Fe mineralogical compositions for Watchtower Class rocks Methusela, Jibsheet, Watchtower, Pequod, and Paros in the Gusev Columbia Hills. These rocks likely have undergone isochemical alteration under low water-to-rock ration conditions because

they have similar chemical compositions but diverse mineralogical compositions ($A_{Ingeous}Fe_T/100$ = 0.78 to 0.08) and Fe oxidations states (Fe^{3+}/Fe_T = 0.43 to 0.94).

Figure 13. $A_{Mt}Fe_T/100$ versus Fe_T for Gusev crater (blue symbols) and Meridiani Planum (red symbols) rock (squares) and soil (circles) samples. The solid line refers to $A_{Mt}Fe_T/100 = Fe_T$. The horizontal dashed lines correspond to values for the saturation magnetization using 92 Am^2/kg for stoichiometric bulk magnetite. Named rocks are Irvine (Ir), Peace (Pe), MimiShoe (MS), Alligator (Al), Tetle (Tt), and Joshua (Jo).

Figure 1.

M_I	M_I	M_I	M_I

Excited State: $\pm 1/2, \pm 3/2$
$\pm 1/2, \pm 3/2$
$\pm 1/2$
$\pm 3/2$
$-3/2$
$-1/2$
$+1/2$
$+3/2$

^{57}Fe Energy Levels

14.4 Kev

Ground State: $\pm 1/2$ $\pm 1/2$ $\pm 1/2$
$+1/2$
$-1/2$

Source (^{57}Co(Rh))	Absorber 1 (Singlet)	Absorber 2 (Doublet)	Absorber 3 (Sextet)
	0 v → v1	0 v → v1 v2	0 v → v1 v2 v3 v4 v5 v6

Schematic MB spectrum and formulas for calculation of MB parameters δ and ΔE

	$\delta = v1$	$\delta = 1/2(v1+v2)$ $\Delta E_Q = v2-v1$	$\delta = 1/4(v1+v2+v5+v6)$ $\Delta E_Q = 1/2((v6-v5)-(v2-v1))$ $B_{hf} = $ (constant)(v6-v1)

Type of magnetic environment	Diamagnetic Paramagnetic or Superparamagnetic	Diamagnetic Paramagnetic or Superparamagnetic	Ferromagnetic Antiferromagnetic or Ferrimagnetic
Representative geological materials with singlet, doublet, and sextet MB spectra	Fe^{2+} in spinel	Fe^{2+} in olivine, pyroxene, ilmenite	Fe^{3+} in hematite, goethite, magnetite Fe^0 in kamacite, Fe^{2+} in troilite

Figure 2

(a) MIMOS II Mössbauer Spectrometer, MB Contact Plate, APXS, MB Temperature Sensor, Robotic Arm, Rock Abrasion Tool (RAT). 1.5 cm. Pancam Image of Spirit's Instrument Deployment Device (IDD) (Microscopic Imager opposite MB)

(b) RAT Grind for MB Targets B032RR (McKittrick_MiddleRAT) and B033RR (McKittrick_MiddleRAT) Burns Outcrop Class Rock. Pancam Image Sol037B_P2533_1_True_RAD

(c) Pancam Image Sol100A_P2544_1_True_RAT. RAT Brush for MB Target A100RB (Route66_SoHo) Adirondack Class Rock

(d) Location for MB Target B046RU (BerryBowl_Empty). Location for MB Target B048RU (BerryBowl_MoessBerry). Pancam Image Sol043B_P2552_1_True_RAD

(e) Pancam Image Sol226A_P2569_1_True_RAD. RAT Grind for MB Target A218RR (Clovis_Plano) Clovis Class Rock

(f) Noseprint for B369SU (TrenchSite_Caviar) Berry Class Soil. Noseprint for B368SU (TrenchSite_RippleCrest2) Berry Class Soil. Noseprint for B367SD (TrenchSite_LeftOf Peanut) Laguna Class Soil. Pancam Image Sol372B_P2374_1_False_L257_pos_2

(g) MB Noseprint for A426SD PasoRobles2_PasoDark) Laguna Class Soil. MB Noseprint for A429SD (PasoRobles2_PasoLight1) Paso Robles Class Soil. Pancam Image Sol431A_P2530_1_True_RAD

(h) MI Image 1M133598293EFF0830P2957M2M1. MB Noseprint for B060SU (MontBlanc_LesHauches) Laguna Class Soil. 1.5 cm. Impressions Made by Temperaure Sensor

Figure 3.

Figure 4.

(a) Rock: A100RB Route66_SoHo — Fe2D1 (Olivine); $(TC/BC - 1)_{MAX} = 0.097$

(b) Rock: A602RU Irvine — Fe2D2 (Pyroxene); $(TC/BC - 1)_{MAX} = 0.105$

(c) Rock: A336RR Wishstone_Chisel — Fe2D3 (Ilmenite); $(TC/BC - 1)_{MAX} = 0.091$

(d) Rock: A568RU Assemblee_Gruyere — Fe2D4 (Chromite), Fe3D5 (Chromite); $(TC/BC - 1)_{MAX} = 0.050$

(e) Soil: A069SU Desert_Gobi — Fe3D1 (npOx); $(TC/BC - 1)_{MAX} = 0.076$

(f) Rock: A493RB LarrysLookout_Paros — Fe3D1 (npOx); $(TC/BC - 1)_{MAX} = 0.064$

(g) Soil: A401SD Pasadena_PasoRobles — Fe3D2 (Fe3Sulfate); $(TC/BC - 1)_{MAX} = 0.106$

(h) Rock: B029RR McKittrick_MiddleRAT — Fe3D3 (Unassigned), Fe3D4 (Jarosite); $(TC/BC - 1)_{MAX} = 0.097$

(i) Rock: B032RR McKittrick_MiddleRAT — Fe3D3 (Unassigned), Fe3D4 (Jarosite); $(TC/BC - 1)_{MAX} = 0.094$

(j) Rock: A376RR Peace_Justice1 — Fe2.5S1 (Magnetite), Fe3S1 (Magnetite); $(TC/BC - 1)_{MAX} = 0.081$

(k) Rock: A213RU+A215RB+A218RR Clovis_Plano — Fe3S3 (Goethite); $(TC/BC - 1)_{MAX} = 0.051$

Data
Fit
TC/BC - 1.0

(l) Soil: B048SU BerryBowl_Moessberry — Fe3S2 (Hematite); $(TC/BC - 1)_{MAX} = 0.054$

(m) Soil: B415SU MattsRipple_Mobarak — Fe3S2 (Hematite); $(TC/BC - 1)_{MAX} = 0.078$

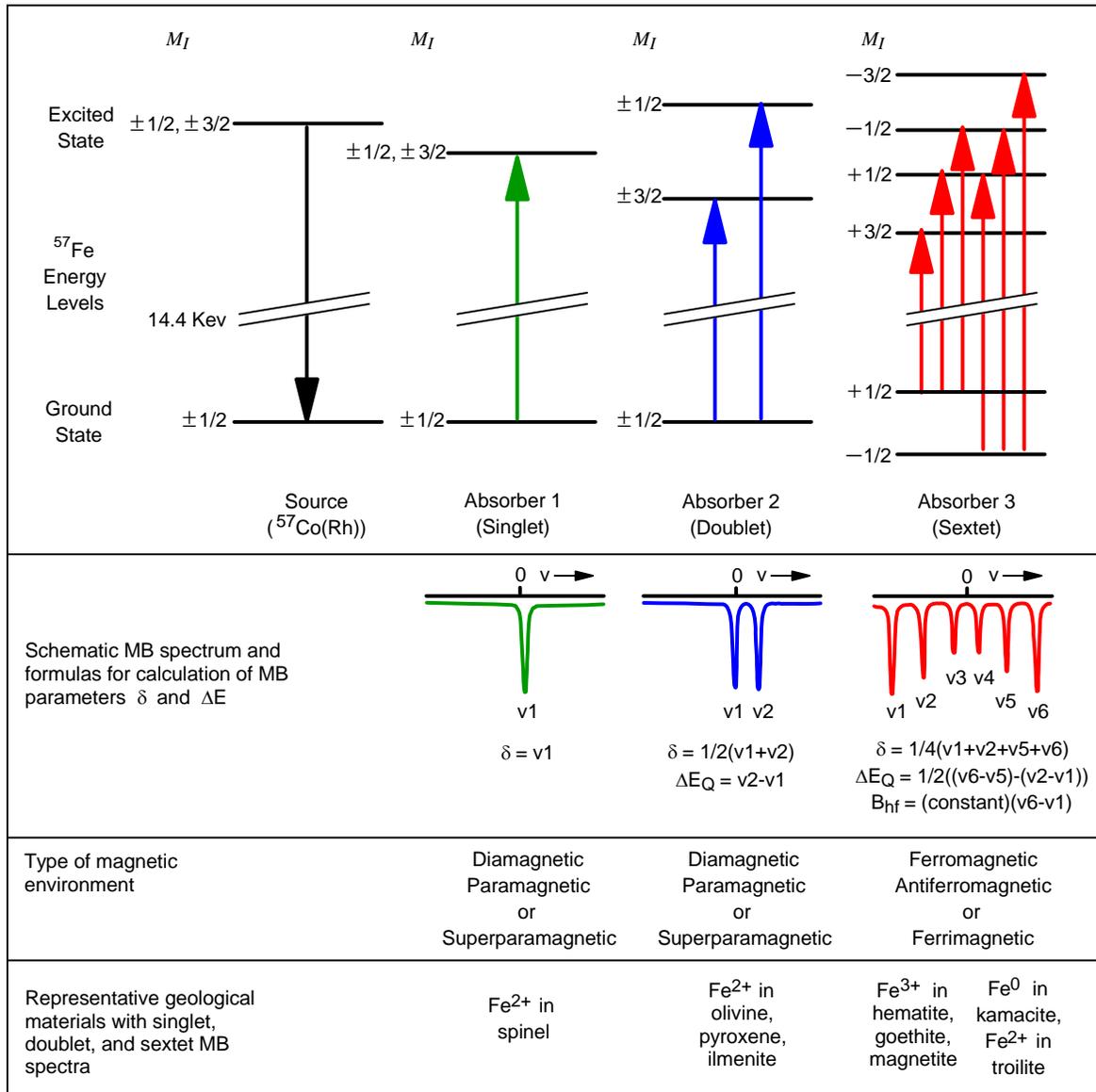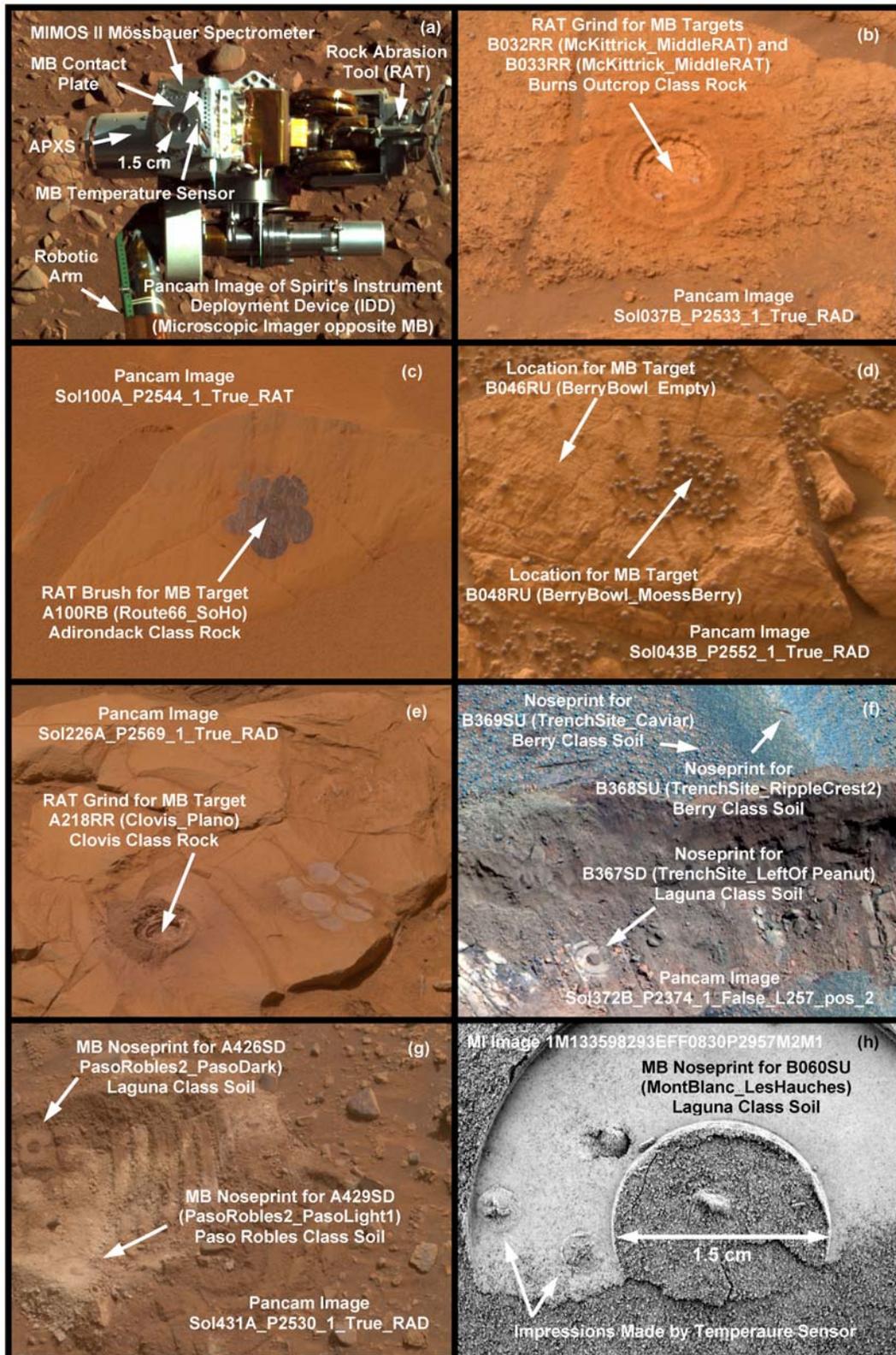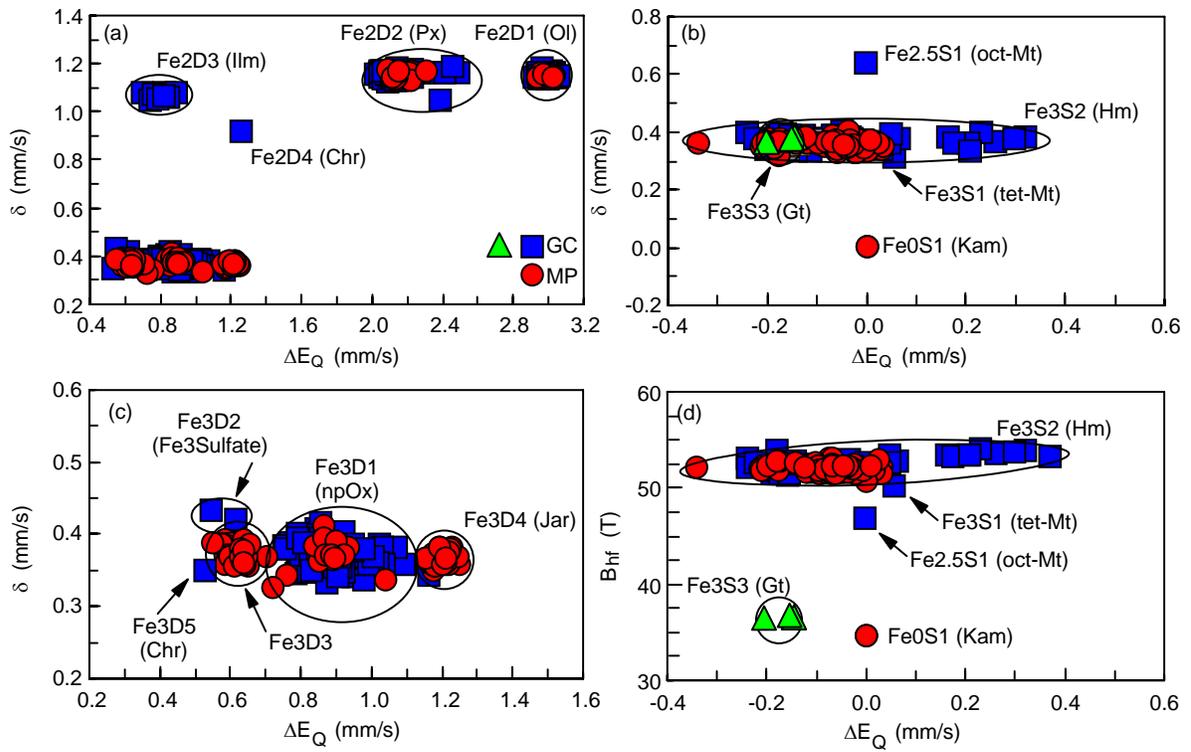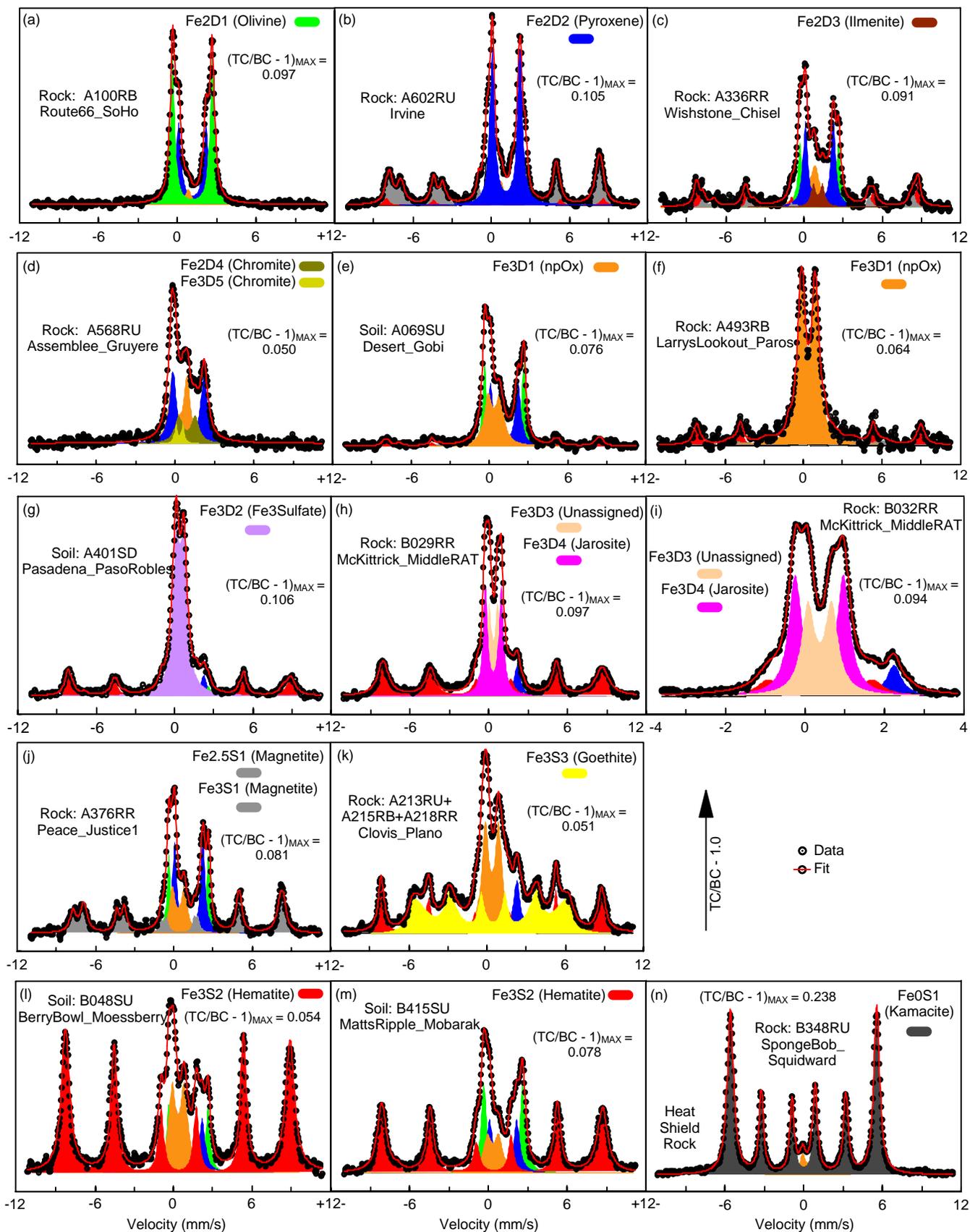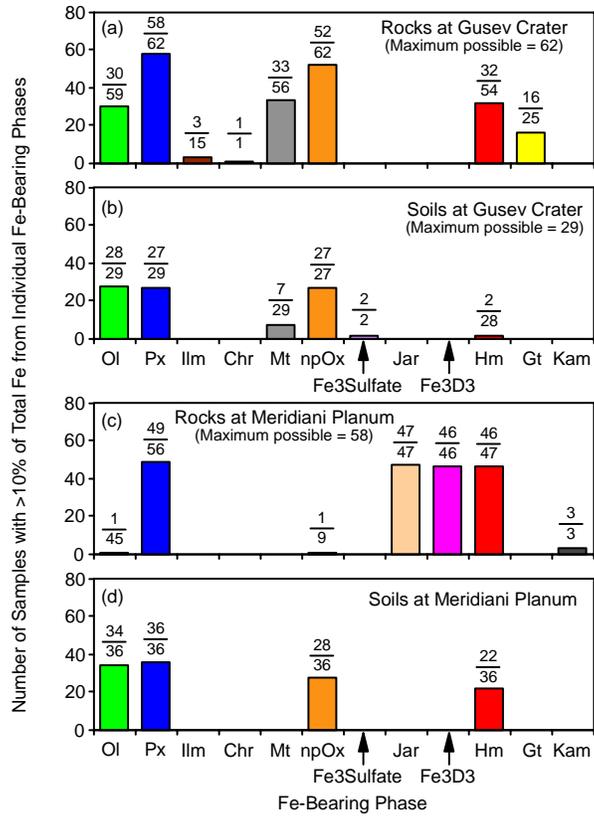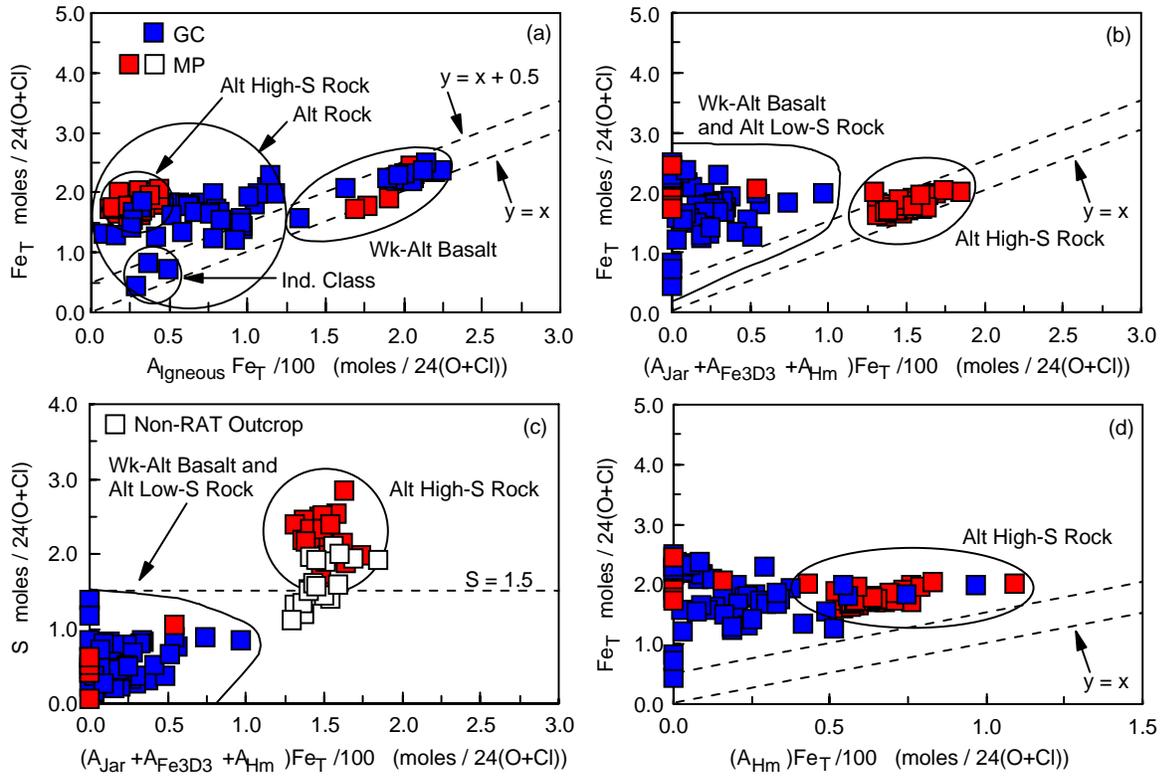(n) Rock: B348RU SpongeBob_Squidward — Fe0S1 (Kamacite); $(TC/BC - 1)_{MAX} = 0.238$; Heat Shield Rock

Velocity (mm/s)

Figure 5.

Figure 6.

Figure 7.

Figure 8

Figure 9

Gusev Crater | **Meridiani Planum**

(a) Weakly Altered Basalt, N = 15, Fe^{3+}/Fe_T = 0.24(11), Ilm = Chr = Fe3Sulfate = Jar = Fe3D3 = Gt = Kam = 0%; Ol = 38(14), Px = 33(5), Mt = 16(12), npOx = 11(5), Hm = 1(1).
Weakly Altered Basalt, N = 3, (Fe^{3+}/Fe_T = 0.01(1)), Ol = Ilm = Chr = Mt = Fe3Sulfate = Jar = Fe3D3 = Hm = Gt = Kam = 0%; npOx = 1(1), Px = 99(1).

(b) Altered Low-S Rock, N = 35, Fe^{3+}/Fe_T = 0.63(18), Fe3Sulfate = Jar = Fe3D3 = Kam = 0%; Gt = 11(12), Ol = 6(8), Px = 24(12), Ilm = 4(7), Chr = 1(4), Mt = 9(7), npOx = 30(14), Hm = 16(12).
Altered Low-S Rock, N = 0, None Analyzed.

(c) Altered High-S Rock, N = 0, None Analyzed.
Altered High-S Rock, N = 20, Fe^{3+}/Fe_T = 0.85(3), Ilm = Chr = Mt = Fe3Sulfate = Gt = Kam = 0%; Hm = 36(3), Ol = 2(1), Px = 14(3), Jar = 29(3), Fe3D3 = 20(2).

(d) Laguna Class Soil, N = 24, Fe^{3+}/Fe_T = 0.30(7), Ilm = Chr = Fe3Sulfate = Jar = Fe3D3 = Gt = Kam = 0%; Hm = 3(2), npOx = 21(7), Ol = 34(5), Mt = 8(2), Px = 33(4).
Laguna Class Soil, N = 10, Fe^{3+}/Fe_T = 0.28(9), Ilm = Chr = Fe3Sulfate = Jar = Fe3D3 = Gt = Kam = 0%; Hm = 4(2), npOx = 20(9), Ol = 33(6), Mt = 6(1), Px = 37(4).

(e) Paso Robles Class Soil, N = 2, (Fe^{3+}/Fe_T = 0.83(5)), Ilm = Chr = npOx = Jar = Fe3D3 = Gt = Kam = 0%; Hm = 14(9), Ol = 7(5), Px = 9(1), Mt = 5(1), Fe3Sulfate = 65(4).
Paso Robles Class Soil, N = 0, None Analyzed.

(f) Berry Class Soil, N = 0, None Analyzed.
Berry Class Soil, N = 13, Fe^{3+}/Fe_T = 0.60(13), Ilm = Chr = Fe3Sulfate = Jar = Fe3D3 = Gt = Kam = 0%; Hm = 44(18), Ol = 18(5), Px = 21(7), Mt = 3(3), npOx = 13(6).

Figure 10

Figure 11

Figure 12

Keystone
(A472RB Keystone_Haunch)

$(A_{Igneous}Fe_T/100 = 0.78; Fe^{3+}/Fe_T = 0.43)$

Gt = 4%
Hm = 15%
npOx = 17%
Mt = 10%
Ilm = 6%
Px = 47%

Keel Davis
(A486RB Keel_Davis)

$(A_{Igneous}Fe_T/100 = 0.42; Fe^{3+}/Fe_T = 0.73)$

Ol = 4%
Px = 13%
Hm = 40%
Ilm = 8%
Mt = 9%
npOx = 27%

Watchtower
(A418RR Watchtower_Joker)

$(A_{Igneous}Fe_T/100 = 0.27; Fe^{3+}/Fe_T = 0.83)$

Gt = 12%
Ol = 7%
Px = 7%
Ilm = 3%
Mt = 1%
Hm = 31%
npOx = 39%

Pequod
(A498RU Pequod_Ahab)

$(A_{Igneous}Fe_T/100 = 0.16; Fe^{3+}/Fe_T = 0.88)$

Gt = 12%
Ol = 4%
Px = 2%
Ilm = 6%
Hm = 14%
npOx = 62%

Paros
(A491RU LarrysLookout_Paros)

$(A_{Igneous}Fe_T/100 = 0.08; Fe^{3+}/Fe_T = 0.94)$

Ol = 3%
Px = 1%
Gt = 11%
Ilm = 2%
Hm = 18%
npOx = 66%

Watchtower Class Rocks
Husband Hill, Columbia Hills
Gusev Crater

Figure 13